Dietary Induced Dynamic Plasticity of Intestinal Stem Cells and the Mucosa in Elevating Risk for Tumor Development

Jiahn Choi[1, ¶], Xusheng Zhang[2, ¶], Wenge Li[1, ¶], Michele Houston[1], Karina Peregrina[1], Robert Dubin[2], Kenny Ye[3], and Leonard H. Augenlicht[1,4, *]

[1] Department of Cell Biology, [2]Genetics, [3]Epidemiology and Population Health, [4]Medicine
Albert Einstein College of Medicine, Bronx, NY

¶These authors contributed equally

***Corresponding Author**
Leonard H. Augenlicht
Professor, Department of Medicine and Cell Biology
Albert Einstein College of Medicine
Ullmann 909
1300 Morris Park Ave.
Bronx, NY 10461
Tel: 718 430-4247
Fax: 718 839-7925
laugenli@montefiore.org

Summary

NWD1, a mouse purified western diet uniquely relevant to human nutritional exposures elevating risk for human sporadic colon cancer rapidly and reversibly altered the stem cell signature and transcriptome of Lgr5^{hi} intestinal stem cells. Down-regulated *Ppargc1a* expression altered mitochondrial structure and function, metabolically reprogramming Lgr5^{hi} cells, suppressing developmental maturation of their progeny as they progress through progenitor cell compartments. This recruited Bmi1+, Ascl2 cells, remodeling the mucosa, including cell adaptation to the altered nutritional environment and elevated pathways of antigen processing and presentation, especially in mature enterocytes, a pathogenic mechanism in human Inflammatory Bowel Disease resulting in chronic low-level pro-tumorigenic inflammation. Plasticity of intestinal cells to function as stem-like cells encompasses a physiological and continual response to changing nutritional environments, supporting historic concepts of tissue homeostasis as a process of continual adaptation to the environment, with important

consequences for mechanisms establishing probability for tumor development. The data emphasize importance of better reflecting human nutritional exposures in mouse models of development and disease.

Introduction:

Dietary patterns are the major driver of risk for sporadic colon cancer (Keum and Giovannucci, 2019), accounting for the vast majority of the disease. Therefore, impact of nutritional risk factors on intestinal stem cells and mucosal homeostasis is fundamentally important (Wei et al., 2017). However, it is well documented that commonly used rodent diets do not establish nutrient exposures reflecting those linked to risk (Augenlicht, 2017b; Li et al., 2019a; Li et al., 2019b; Peregrina et al., 2015; Bastias-Perez et al., 2020; Speakman, 2019) and Discusson). The importance of this disconnect is illustrated by the fact that mouse intestinal stem cells reach crypt clonality in 6 weeks, but it takes 6 years - 50 times longer - in humans (Hodder et al., 2018; Nicholson et al., 2018; Shivdasani, 2021), likely due to the different nutritional environments of mouse and humans (Hodder et al., 2018; Nicholson et al., 2018; Shivdasani, 2021). Thus, though modeling complexity and variability of the human diet is a major challenge, the necessity to better reflect human nutritional exposures in the mouse is no different from the well-accepted mandate that recapitulating human genetic alterations and regulatory networks in mouse models is fundamental for understanding etiology and mechanism of human disease.

Therefore, we have used a novel purified western-style diet (NWD1) to better reflect nutritional exposures causing risk for human intestinal tumors. Formulated on the principal of nutrient density, NWD1 adjusts exposure for the mouse of key nutrients each at its level linked to higher risk for human CRC (Newmark et al., 2001). NWD1 is highly pro-tumorigenic, amplifying intestinal tumor phenotype in mouse genetic models regardless of genetic drivers (Yang et al., 1998; Yang et al., 2008b; Yang, 2003; Yang et al., 2001). Most important, wild-type mice fed NWD1 are the only model that develops sporadic colon and intestinal tumors, with

the etiology, incidence, frequency and lag with age of human sporadic colon cancer (Aslam et al., 2010; Newmark et al., 2001; Yang et al., 2008a). Thus, data from NWD1 mice are relevant to mechanisms establishing risk for most human colon cancer.

NWD1 fed mice are not obese, maintain calcium levels and bone mineral density, and reflect human metabolic syndrome: reduced energy expenditure without altered food consumption or physical activity, causing glucose intolerance, and increased pro-inflammatory cytokines (Bastie et al., 2012). NWD1 reduces intestinal Lgr5^{hi} cell lineage tracing, their mutation accumulation, and efficiency in tumor initiation, increasing these for an alternate stem cell population (Augenlicht, 2017a; Li et al., 2019a; Li et al., 2019b; Newmark et al., 2009; Peregrina et al., 2015; Wang et al., 2011; Yang et al., 2008a) consistent with the expanded proliferative compartment in NWD1 mice (Newmark et al., 1990; Newmark et al., 1991), recapitulating well-documented expansion of this compartment in humans at environmental or genetic risk (Lipkin et al., 1983; Lipkin and Newmark, 1985; Lipkin et al., 1981b).

Here we establish NWD1, in dramatically reprogramming Lgr5^{hi} stem cells, down-regulates *Ppargc1a* expression, a master regulator of mitochondrial biogenesis, altering mitochondrial structure and function and metabolically reprogramming the cells, recapitulated by *Ppargc1a* genetic inactivation in Lgr5 cells. Single cell RNAseq analysis of both the NWD1 model and the *Ppargc1a* genetic knockout mice, coupled with novel cell trajectory branch point analysis, demonstrate the altered metabolic programming suppresses developmental maturation of stem cell progeny as they transit through progenitor cell compartments. As a consequence, Bmi1+, Ascl2^{hi} cells above the crypt base are mobilized to maintain the mucosa, but remodel lineages to adapt to the nutritional environment. This also elevated pathways of antigen presentation and processing, a pathogenic mechanism establishing pro-tumorigenic chronic inflammation in human inflammatory bowel disease (de Jong et al., 2001; Ishigami et al., 2001; Lawrance et al., 2001), (Beswick and Reyes, 2009; Xia et al., 2005), with inflammation also seen in the NWD1 model.

The rapidity and reversibility of programming with dietary shift establish that plasticity of intestinal epithelial cells to assume stem cell functions is not solely a damage response to restore homeostasis (Murata et al., 2020; Shivdasani et al., 2021) but also encompasses rapid response to dietary changes. The data support historic concepts of the *"milieu interiuer"* of Claude Bernard in the 1800's, and Cannon's coining of the term homeostasis in the 1940's (Davies, 2016), each emphasizing homeostasis not as a state, but a process of continual tissue adaptation to changing environments. Thus, the mucosa is in constant flux in response to nutrients, with competitive advantages that oncogenic mutations provide to stem cells (Shivdasani, 2021) carried out on a playing field metabolically and physiologically sculpted by the nutritional environment.

Results:

NWD1 Impact on Lgr5^{hi} cells: Bulk RNAseq analyzed Lgr5^{hi} cells from *Lgr5$^{EGFP\text{-}creER}$* mice fed NWD1 or AIN76A control diet for 3 or 12 months from weaning (**Fig1a**: Arms 1,2), or 3 months NWD1 then switched to AIN76A and sacrificed at 12 months (Arm 3 –crossover). >95% of Lgr5^{hi} stem cell signature genes (Munoz et al., 2012) were down-regulated at 12 versus 3 months, regardless of diet (**Fig 1B,C**). Within this down-regulation, NWD1 elevated expression of 78 sequences at 3 months, 73 also up-regulated at 12 months (**Fig 1D**). In the crossover Arm 3, 64 of 73 sequences up-regulated at 12 months (88%) reverted towards expression in AIN76A fed mice (**Fig1D**). NWD1 down-regulated 15 Lgr5^{hi} cell signature genes at 3 months, most not persisting to 12 months, with no effect of dietary crossover (**Fig 1D**).

For the Lgr5^{hi} cell transcriptome (~8,000 genes), NWD1 elevated and decreased expression of 164 and 63, respectively, at 3 months **(Fig 1D**), increasing 4-fold at 12 months to 551 and 229 (**Fig 1D**), and reverted to more limited perturbation by dietary cross-over (**Fig 1D**).

By gene set enrichment analysis (GSEA), NWD1 up- and down- regulated 25 and 30 pathways at 3 months, key pathway changes persisted to 12 months, and reverted to control levels in the cross-over arm (**Fig 1E,F)**. Up-regulated DNA mismatch, base excision and

nucleotide excision repair (**Fig 1E**) are associated with decreased Lgr5^{hi} cell mutation accumulation (Li et al., 2019b). NWD1 repressed TCA cycle and oxidative phosphorylation (Oxphos) (**Fig 1F**), reversed by shift to AIN76A. The significance is that fatty acid oxidation and intact mitochondrial function are necessary for intestinal, hematopoetic and embryonic cells to function as stem cells (Chen et al., 2020; Ito et al., 2012; Khoa et al., 2020; Koehler et al., 2017; Rodriguez-Colman et al., 2017). Therefore, down-regulated Oxphos and TCA cycle can drive the NWD1 suppression of Lgr5^{hi} cell lineage tracing and tumor initiation. NWD1 down-regulated 58 of 132 genes in the Oxphos pathway at 3 months (**Fig 2A**), encompassing multiple subunits of each mitochondrial electron transport chain complex (**Fig 2B**), confirmed by interrogating data from an independent cohort of 3 month fed mice (Li et al., 2019b) (**Fig 2A**). Greatest down regulation in both cohorts were *Cox6a2* and *Cox7a1* of cytochrome oxidase, the terminal respiratory chain enzyme, and *Sdhb*, and *Sdhd* of complex II, succinic dehydrogenase (**Fig 2A,C**). These are down-regulated in CRC and other cancers causing succinate accumulation and tumor development (Bardella et al., 2011; Zhang et al., 2013). Mean decreased Oxphos gene expression was 14% and 11% in the two data sets **(Fig 2A),** reflecting the high significance for GSEA negative enrichment**,** and persisted at 12 months (65 of 67 genes (97%) decreased by a mean of 10% (**Fig 2D**). In crossover to control diet (Arm 3), 52 (82%) of down-regulated genes increased towards control levels (**Fig 2D**), reflecting GSEA reversal (**Fig 1F**). In comparison to changes in the 8,000 expressed gene set, NWD1 Oxphos gene down-regulation was significant ($P=10^{-26}$, Fisher's exact test) and also for genes up-regulated when switched back to AIN76A ($P=10^{-18}$).

NWD1 reduced Lgr5^{hi} cell *Ppargc1a* expression by ≥60% in both cohorts (**Fig 3A,C**), persisted to 12 months and reversed by dietary crossover (**Fig 3B**). *Ppargc1a* encodes Pgc1a, a key regulator of metabolism and mitochondrial biogenesis (Puigserver and Spiegelman, 2003; Wu et al., 1999), with overexpression elevating mitochondrial biogenesis and function and altering cell fate of colonic epithelial cells (D'Errico et al., 2011). NWD1 down-regulated Pgc1a

protein in crypt base cells, but with no change in villus cells above the crypt base (**Fig 3D,E**), and no alteration in *Ppargc1a* expression in isolated Bmi1+ cells throughout the mucosa (**Fig 3F**). NWD1 decreased mitochondria cristae density in crypt base columnar cells (**Fig 3G,H**), paralleling NWD1 suppressed Lgr5 CBC cell lineage tracing (Li et al., 2019a; Peregrina et al., 2015), but there was no change in cristae density in crypt Paneth cells or villus cells (**Fig 3H).** Lgr5^{hi} GFP marked cells decreased 60% in NWD1 mice (*P=0.03*, **Fig 3I,J,K)** and staining of Lgr5^{hi} GFP cells with Mitotracker red, an index of mitochondrial function, decreased (*P<0.0001*; **Fig 3L**).

Ppargc1a was inactivated in Lgr5^{hi} cells hetero- and homozygously in control diet fed *Lgr5*$^{EGFP\text{-}cre:ER\text{-}}$, *Ppargc1a*$^{loxp/loxp\ or\ loxp/+}$, *Rosa26*^{tom} mice. Homozygous *Ppargc1a* inactivation phenocopied NWD1 effects: Lgr5+ cell lineage tracing was suppressed (**Fig 4A,B,** *P=0.02*), and CBC cell cristae density decreased with no alteration in Paneth or villus cells (**Fig 3G,H**). Thus, NWD1 down-regulation of *Ppargc1a* contributes to NWD1 suppression of Lgr5^{hi} stem cell function.

Single cell (sc)RNAseq analyzed FACs isolated intestinal epithelial cells (Epcam+, CD45neg) from mice 3 days after Lgr5 cell *Ppargc1a* inactivation. Twenty cell clusters were aligned by marker expression with intestinal cell types and all lineages (**Fig S1A,B**). A minor cluster could not be aligned (UK; <1% of cells in any single cell library). Cell proportion in each cluster was similar for all genotypes, but with a progressive increase of EC1 and EC2 cells with het and hom inactivation (**Fig S1B**). Trajectory analysis placed EC1 proximal to Dividing cells, with EC2 emerging on that trajectory, and other EC cells and lineages arising further down-stream (**Fig 4C**), the predicted progression consistent with markers identifying cell position along the crypt-villus axis (**Fig S1C,** (Moor et al., 2018)). Therefore, altered EC1 and 2 cell number proximal to progenitor cells was consistent with the short 3 days between *Ppargc1a* genetic inactivation and scRNAseq analysis.

Oxphos is necessary for stem cell functions, and mitochondrial function also can determine whether stem cells retain self-renewal capacity or differentiate (Iwata et al., 2020). Therefore, progression of immature cells through progenitor cell compartments was investigated. At branch point "a", developmental trajectory from the Replicating 1 cell compartment (R1) bifurcates to secretory goblet cell lineages or R2 cells (red arrow, **Fig 4C**). For WT and *Ppargc1a* het mice, R1 cells were the major cell type at point "a" with few or no Stem cells (**Fig 4D,E**), indicating transition from Stem to R1 when cells reached this early branching point. However, with homozygous *Ppargc1a* inactivation, 100% of cells at "a" were Stem cells, a major repression of the re-programming with maturation from Stem to R1 cells ($P=10^{-5}$, by a weighted linear regression based on cell number at each cluster for each mouse). Altered cell distribution at branch "a" with hom inactivation was paralleled by suppression of Oxphos, TCA cycle, cell cycle, and glycolysis pathways (**Fig 4F**), demonstrating metabolic reprogramming, but these were not altered in het inactivated mice, paralleling absence of change in cell type distribution.

With further cell maturation, branch point "b" was transition from R2 to enteroendocrine and Tuft cells (**Fig 4C**). At "b", most cells in WT or het mice had progressed to R2, but with homozygous *Ppargc1a* inactivation, 90% remained in R1 (**Fig 4G,H,I**; *P=0.016*), with repression of the Oxphos pathway. Therefore, homozygous *Ppargc1a* inactivation altered Stem cell transition to R1 cells, and repressed transition out of R1, linked to down-regulation of the Oxphos pathway and repressed lineage tracing overall, as was effect of NWD1 on Lgr5^{hi} stem cells.

Rapidity of dietary alterations: scRNAseq analyzed intestinal epithelial cells of mice fed AIN76A for 3 months (**Fig 5A**, Arm 1), these mice switched to NWD1 for 4 days (Arm 2), and the 4d NWD1 mice switched back again to AIN76A for 4 days (Arm 3). Stem, replicating, dividing cells and all lineages were identified**,** with no significant changes in cell distribution for clusters among the 3 arms. However, there was a bias towards increased Stem, R, and Dividing cells in Arms 2 and 3 consistent with the short time frame of dietary alteration (**Fig S2A,B**). For

the stem cell cluster, 4 days of NWD1 altered 30 pathways (*P=10*$^{-3}$ *to 10*$^{-45}$) including repression (negative Z-score) of the TCA cycle and Oxphos (**Fig 5B,C**): 19 of the 30 pathways reverted to control values in 4d NWD1 mice switched back to AIN76A for 4 days, including the TCA cycle, but not Oxphos (**Fig 5C**). Thus, 8 genes encoding TCA cycle enzymes were down-regulated by 4d NWD1 switch and reversed by 4d switch-back to AIN76A (**Fig 5D**), reflecting the significant GSEA for dietary shifts (**Fig 5B.C**). However, while 4d of NWD1 decreased expression of 51 Oxphos pathway genes, reflecting the significant negative enrichment, only 15 of these reversed on switch back to AIN76A, reflecting lack of significant reversal (**Fig 5B,C; Fig S3**).

Trajectory analysis of cell maturation for rapid dietary shifts, consistent with markers for cells along the crypt-villus axis (**Fig S2C),** identified three early branch points (**Fig 5E**). In AIN76A mice, 80% of cells at branch point "a" were Stem cells and 20% R, but after 4d switch to NWD1, Stem cells increased to 100% with no R cells (**Fig 5F,G**), approaching significance (*P=0.068*), paralleled by significant negative enrichment for Oxphos, DNA replication and cell cycle pathways (**Fig 5H**). 4d switch back to AIN76A did not reverse the decreased Oxphos pathway, but did reverse DNA replication and Cell Cycle pathways, favoring progression of cell maturation from the Stem cell compartment (**Fig 5G**). Branch point "b" was bifurcation of maturing cells to R or dividing cells (**Fig 5E**): 100% of cells were R with no Div cells in AIN76A mice (**Fig 5I,J**) shifting to 90% R, 10% Div by 4d NWD1, but changing back to AIN76A did not shift this, with further decreases. These patterns were not statistically significant, but were concomitant with highly significant decreased Oxphos, DNA replication, glycolysis and the TCA cycle by 4d of NWD1 feeding, but only glycolysis and the TCA cycle significantly reversed by switching back to AIN76A, consistent with the critical role of metabolic state as a determinant of cell maturation (**Fig 5K**). There were no differences at branch point "c" with rapid dietary shifts, a point between secretory and absorptive cell differentiation, consistent with the short time frame precluding cells reaching branch point "c" (**Fig S4**).

Therefore, rapid dietary shifts induced rapid, significant metabolic re-programming of cells in their progressive maturation through progenitor cell compartments, but cell programming changes at branch points were less robust than those induced by *Ppargc1a* inactivation, suggesting a longer time frame for dietary shifts in cell identity to accumulate. This becomes clear in Bm1+ cells mobilized by the NWD1.

NWD1 mobilization of Bmi1+ cells: Despite repressed Lgr5^{hi} stem cell function, Western-style diets expand the mouse intestinal proliferative cell compartment (Newmark et al., 1990; Newmark et al., 1991), recapitulating expansion in humans at elevated CRC risk (Lipkin et al., 1983; Lipkin et al., 1989; Lipkin and Newmark, 1985; Lipkin et al., 1981a). This suggests NWD1 mobilizes cells above the crypt base, and NWD1 induced lineage tracing from Bmi1+ positive cells above the crypt base, persisting for months (Li et al., 2019b; Peregrina et al., 2015). Moreover, tumor development following targeting *Apc* inactivation to Bmi1+ cells was increased by feeding NWD1, paralleling their NWD1 induced lineage tracing acquisition (Li et al., 2019a; Li et al., 2019b).

Mucosal Bmi1+ cells encompass multiple epithelial cell types, some induced by Lgr5^{hi} cell damage to dedifferentiate to reconstitute the stem cell compartment (Murata et al., 2020; Shivdasani, 2021). To dissect dietary impact on Bmi1+ cells, these cells and their marked epithelial cell progeny were isolated from *Bmi1$^{cre\text{-}ERT2}$, Rosa26^{tom}* mice fed diets for 3 months from weaning (Tom+, Epcam+, CD45neg), at 3 days after Tam injection (shorter), or after marked cells accumulated for 66-70 days after Tam (longer) (**Fig 6A**). scRNAseq identified stem, replicating, dividing, and all cell lineages (**Fig S5**), with similar cell distributions among cell types regardless of diet (**Fig 6B**). Therefore, despite NWD1 repressing Lgr5^{hi} stem cell functions, the mucosa was maintained.

Trajectory analysis, consistent with markers identifying cells along the crypt-villus axis (**Fig S5C**), predicted two main branches for enterocyte and secretory cells arising from stem, replicating and dividing cells, similar regardless of diet or time post Tam marking (**Fig 6C**).

Expression of the stem cell transcription factor Ascl2 causes dedifferentiation of Bmi1+ cells to replace damaged Lgr5^{hi} cells (Murata et al., 2020; Shivdasani, 2021). Regardless of diet or time post Bmi1+ cell marking, *Ascl2* expression was most abundant in Stem1 and 2, Replicating and Dividing cells (**Fig 6D** blue arrows**,E,F**). A small number of Tuft and goblet cells also expressed *Ascl2* where goblet and enteroendocrine lineages diverged (**Fig 6D,** orange arrows, and **6E**).

Among progenitor cells, *Ascl2* expression was highest in Stem2 (**Fig 6F**), with expression per cell heterogeneous, unlike for Stem1, R, or Div cells (**Fig 6G**). A subset of Stem2 cells in NWD1 mice longer term after marking expressed higher *Ascl2* (**Fig 6G,** red arrow), a pattern highly significant by multiple tests (Methods).

Ascl2^{hi} expressing cells were confined to the crypt base in AIN76A mice (**Fig 6H**), but in NWD1 mice, elevated *Ascl2* was in cells above the crypt base that co-expressed Bmi1+ (**Fig 6H**), as in mice after acute Lgr5^{hi} cell damage (Murata et al., 2020; Shivdasani, 2021)

There are 2 early trajectory branch points among progenitor cell populations (**Fig 6C**, red arrows). At branch point "1", Stem1 cells give rise to secretory lineages. In AIN76A mice, 80% of branch point "1" cells were Stem1, with 20% Stem2 in short term marked cells, but for NWD1 fed mice 100% of cells were Stem1 (**Fig 6I**). Longer term after marking (66-70d post Tam), all cells at branch point "1" were Stem1 cells regardless of diet. At branch point "2", Stem1 cells diverged to Replicating and Dividing cells (**Fig 6C**). Shorter term after marking, for AIN76A mice, branch 2 cells were equally distributed between R and Div cells, but longer term, shifted to 10-20% R and 80-90% Div. However, for mice fed NWD1 either shorter or longer term, 100% of cells at branch 2 were R cells (**Fig 6I**). Dietary differences at branch point 2 were highly significant longer and shorter term after cell marking (*P=0.001*). Bmi1+ cells in R longer term after marking express much higher Ascl2 levels (**Fig 6J;** $P=10^{-8}$). These R cells, predicted to produce Stem2 cells, thus already express *Ascl2* at high levels, similar to the Stem2 subset in

NWD1 mice longer term after marking (**Fig 6G**), and may be their direct precursors accumulating in the NWD1 mice (**Fig 6H**).

NWD1 Impact on enterocytes: NWD1 altered expression profiles in all Bmi1+ cell populations both long and short term after marking, most pronounced in enterocytes, and greatest in EC7 enterocytes accumulating longer term (**Fig 7A**). EC7 is predicted to be the most mature enterocyte cell population (**Fig 6C**), confirmed by markers that identify villus tip cells ((Moor et al., 2018), **Fig S5B,C**, arrows).

The EC7 cell pathway most extensively enriched by NWD1 mediates antigen processing and presentation (**Fig 7B,C**). CD74 in this pathway is expressed in epithelial cells (Beswick and Reyes, 2009; Biton et al., 2018; Collins et al., 1984; Gold et al., 2010; Ishigami et al., 2001; Jiang et al., 1999; Momburg et al., 1986; Schroder, 2016; Tamori et al., 2005; Volc-Platzer et al., 1984), and in mouse Lgr5^{hi} stem cells, mediates interaction between stem cells and their immune environment (Biton et al., 2018). CD74 interacts with proteins of the major histo-compatability II (MHCII) complex to process and present cell surface antigens (Schroder, 2016), and MHCII complex genes were also upregulated in EC7 cells (**Fig S6**). The percent of cells expressing CD74 in this pathway was elevated in every Bmi1+ cell cluster accumulating longer term (**Fig 7D**), but the much greater increase in level of expression per cell for EC7 cells was highly significant (**Fig 7E**; $P=10^{-25}$, by negative binomial regression analysis), consistent with reported expression of the CD74/MHCII complex predominantly in cells in the upper third of villi (Wosen et al., 2018), suggesting a unique role in these differentiated cells,

Cell surface expression of CD74 characterizes dysplastic cells of the intestinal epithelium, and cells of Crohn's, Ulcerative, and Amebic colitis in the human (de Jong et al., 2001; Ishigami et al., 2001; Lawrance et al., 2001), with chronic inflammation in each linked to elevated CRC risk. NWD1 is also pro-inflammatory, elevating serum levels of inflammatory cytokines (Bastie et al., 2012), and there was a 2-3 fold increase in cells expressing CD3, a pan T cell marker, in

3 month NWD1 compared to AIN76A mice, significant when quantified by CD3 cells/villus (*P=0.008*), or percent area/villus epithelial column expressing CD3 (*P=0.015*) (**Fig S7A,B,C**).

The second most highly enriched pathway in EC7 cells in NWD1 is "Intestinal Immune Network/IgA production" (**Fig 7B,C**). IgA is abundant in the intestinal and colonic mucosa, modified as it traverses into and out of the lamina propria to form an SIgA complex interacting with the FcαRI receptor on myeloid cells, which is pro-inflammatory. F/480+ myeloid cells in the mucosa were also elevated by NWD1 (*P=0.010*; **Fig. S7D,E**), also characterizing pro-tumorigenic IBD (Breedveld and van Egmond, 2019).

The next three most highly enriched pathways in EC7 cells are *Ppar* signaling, cholesterol metabolism, and fat digestion/absorption (**Fig. 7B,C**), adaptive responses to increased fat (25%) in NWD1. With rapid dietary cross-over (**Fig. 5A**), fatty acid metabolism was elevated in all cell clusters after the 4 day switch to NWD1 from AIN76A, and except for Goblet2 and EE2, reverted for the clusters within 4 days of switch back to AIN76A (**Fig. 7F**), consistent with rapid shift of metabolic pathways (**Fig 5**). A second adaptive response was increased *Trpv6* in enterocytes of 3-month NWD1 fed mice, shorter and longer term after Bmi1+ cell marking (**Fig. 7G**). *Trpv6* encodes the enterocyte brush border calcium channel, mediating calcium uptake under low dietary calcium conditions (Suzuki et al., 2008). Therefore, elevated *Trpv6* expression is how NWD1 mice maintain serum calcium levels (Bastie et al., 2012), despite lower calcium and vitamin D_3 in NWD1. Thus, lineages adapted to nutritional environments rapidly.

Discussion:

Rapidity and reversibility of NWD1 altered stem cell signature genes and Lgr5^{hi} cell expression profile overall establish that nutrient exposures impose continual flux on how cells function as intestinal stem cells, with important implications. First, cells cycling among states impacts mutation and epigenetic alterations and their penetrance, and NWD1 decreased Lgr5^{hi} cell mutation accumulation while increasing mutational burden from the expanded Bmi1+ cell population (Li et al., 2019a; Li et al., 2019b). Second, epigenetic "history" of a cell dictates its

future course and responses to signals (Gonzales et al., 2021). Third, impact of onco- and tumor suppressor genes and key regulators are always context dependent, with major differences in the role and regulation of such genes among tissues and lineages in both normal functioning and as drivers of disease. Indeed, adjusting dietary vitamin D or calcium altered Lgr5^{hi} cell expression profile, but altered profile was dependent on the overall dietary context in which these specific nutrients were changed (Li et al., 2019b). In this regard, adjusting individual components of NWD1, or feeding high fat diets, do not reproducibly cause mouse sporadic tumors, but the combination of nutrient adjustments in NWD1 does. Thus, capturing complex nutrient interactions, while challenging, is fundamental (Steck and Murphy, 2020).

NWD1 rapidly and persistently down-regulated *Ppargc1a* in Lgr5^{hi} cells repressing the Oxphos and TCA cycle pathways, recapitulated by genetic inactivation of Lgr5 cell *Ppargc1a*, and in both cases repressed the developmental maturation of stem cell progeny as they progressed through progenitor cell compartments. The fundamental significance of this is emphasized by necessity of Oxphos for mouse Lgr5^{hi} and Drosophila intestinal stem cells to function as stem cells (Chen et al., 2020; Rodriguez-Colman et al., 2017; Koehler et al., 2017), for hematopoietic stem cell functions (Ito et al., 2012), for embryonic stem cell pluripotency (Khoa et al., 2020), and role of mitochondrial function in determining whether stem cells self-renew or differentiate (Iwata et al., 2020).

NWD1 elevated *Ascl2* expression in a Bmi1+ cell population above the crypt, a stem cell transcription factor essential for Bmi1+ cell dedifferentiation in response to Lgr5^{hi} cell damage (Murata et al., 2020; Shivdasani, 2021). Ascl2 is regulated by Wnt signaling (Schuijers et al., 2015), which is elevated by NWD1 throughout cells of the intestinal villi and the colonic mucosa (Augenlicht et al., 1991; Wang et al., 2011; Yang et al., 2008a). However, the role of Bmi1+, Ascl2^{hi} cells likely differs in dietary versus damage induced plasticity. Acute damage purges Lgr5^{hi} crypt base stem cells, with *Ascl2* mobilized cells migrating into the crypt, restoring crypt organization. However, limited crypt space establishes competition among crypt Lgr5^{hi} cells

(Shivdasani, 2021), and single cell laser ablation of crypt base cells triggers division and reorganization of remaining stem cells, confirming importance of physical space in stem cell dynamics (Choi et al., 2018). In contrast, with chronic NWD1 feeding, crypt space may be limited for replacement cells, and Lgr5^{hi} stem cells migrating into the niche would still be repressed by NWD1. Potential selection for repopulating cells resistant to NWD1 repression is unlikely, since reduced Lgr5^{hi} cell lineage tracing, and Oxphos and TCA pathway repression, persist to at least 1 year of feeding NWD1(Peregrina et al., 2015) (and figure 1F), and marked Bmi1+ cells above the crypt base lineage trace for months in mice continuously fed NWD1(Li et al., 2019b).

NWD1 altered expression profiles of all lineages, most extensively in mature, villus tip EC7 enterocytes, with the greatest change elevation of CD74 and MHCII pathways that interact in processing and presenting antigens to the cell surface. A 60% fat diet repressed these pathways in Lgr5^{hi} cells, suggested to be pro-tumorigenic by dampening immune surveillance (Beyaz et al., 2021). The contrasting results in the NWD1 and 60% fat diet models can be due to: first, substantial differences in dietary formulation; second, the dependence of pathway repression by 60% dietary fat on mouse microbiome composition, differing significantly among mouse rooms at the same institution (Beyaz et al., 2021), and likely different among institutions and with different diets; third, NWD1 pathway elevation is in cells derived from mobilized *Bmi1+, Ascl2^{hi}* cells, not a feature of the 60% fat model, with the interesting possibility that response may be a function of stem cell of origin. Most important, however, the NWD1 increase in these pathways recapitulates results in humans, with highest expression reported in the upper villi of the human small intestine (Wosen et al., 2018). Moreover, NWD1 increased pro-inflammatory cytokines (Bastie et al., 2012), and CD3 and myeloid cell mucosal infiltration, paralleling elevation of the CD74/MHCII pathway in human Crohn's, Ulcerative, and Amebic colitis, (de Jong et al., 2001; Ishigami et al., 2001; Lawrance et al., 2001), confirmed by single cell analysis of human IBD tissue (Parikh et al., 2019), and also in H.pylori infected gastric tissue (Beswick

and Reyes, 2009; Xia et al., 2005). Each arevchronic inflammatory states increasing risk for human tumor development. Extending the parallel, NWD1 altered CD74 expression most extensively in mature EC7 cells, similar to upper crypt colonocytes exhibiting greatest increase in IBD (Parikh et al., 2019), and NWD1 induces high ectopic expression of Lyz and other Paneth cell markers in mouse colon (Wang et al., 2011), similar to Lyz elevation in human IBD tissue (Parikh et al., 2019).

Thus, stem cell functions and homeostasis in NWD1 mice differ from reports on mice fed commonly used diets, but such diets do not reflect human nutrient exposures. For example, 60% fat diets modeling obesity greatly exceed fat consumed by even obese humans, inducing mouse metabolic alterations different than those induced by 45% fat also causing obesity but better reflecting fat consumption of humans at higher CRC risk (Bastias-Perez et al., 2020; Speakman, 2019). Additionally, all commonly used mouse diets, including 60% fat diets, establish mouse vitamin D_3 levels representing “zero” per cent of the human population: 200-300% higher than the population mean, 500% higher than levels linked to higher risk for CRC, and ~50% higher than the highest level in only 1% of the population (Augenlicht, 2017b; Li et al., 2019a; Li et al., 2019b; Peregrina et al., 2015). This is fundamental: $Lgr5^{hi}$ cell vitamin D receptor (Vdr) expression is down-regulated in $Lgr5^{lower}$ daughter cells leaving the stem cell niche (Munoz et al., 2012), suggesting Vdr requirement for $Lgr5^{hi}$ stem cell function, as in hair follicle stem cells (Demay et al., 2007). Further, lower vitamin D_3, or Lgr5 cell *Vdr* inactivation, reduces Lgr5 cell lineage tracing, concomitantly decreasing their tumor initiating efficiency (Li et al., 2019a; Li et al., 2019b; Peregrina et al., 2015). Therefore, mice fed common diets likely do not reflect the complexity of how and which intestinal stem cells function in humans, contributing to the fact that crypt stem cell clonality takes about 50 fold longer in humans than in mice (Hodder et al., 2018; Nicholson et al., 2018; Shivdasani, 2021).

Nutrient induced field effects are a hallmark in prevention research (Lochhead et al., 2015), interactive with oncogenic mutations, such as the parallels between altered lineage tracing from Lgr5^{hi} and Bmi1+ cells in mice fed different diets and their altered efficiencies in initiating tumors (Li et al., 2019b; Peregrina et al., 2015). Further, in clonal hematopoiesis and leukemia, extrinsic factors influence the fluctuating outgrowth of dominant clones with oncogenic mutations (Stauber et al., 2021).

Tumors reflect successful growth advantage of transformed cells (Shivdasani, 2021), but this is very rare: lower-risk individuals develop no sporadic tumors, but those at higher risk, only 1-2 despite many billions of mucosal cell divisions over decades, suggesting mechanisms establishing risk are subtle and complex. Therefore, it is fundamental that the nutritional environment dynamically and continually sculpts the playing field on which intestinal stem cell competition takes place.

Experimental Procedures:

Mice: Mice, all on a C57Bl/6J background, were provided food and water *ad libitum* in a barrier facility at the Albert Einstein College of Medicine. For breeding, strains were fed a chow diet (Picolab 5058, Fisher Feed, Branchburg, NJ). Genotyping was by PCR of DNA from tail clips at 5 days following birth, using published primers and methods. Appropriate genotypes were randomized to purified diets (AIN76A, D10011; NWD1, D16378C; Research Diets Inc, New Brunswick, NJ). Mice of both genders were used (a total of 25 male and 20 female mice). Tamoxifen in corn oil was given as a single injection (Sigma, T5648, 100µl, 1mg/µl). Experiments were approved by the Albert Einstein Institutional Animal Care and Use Committee.

Isolation of intestinal epithelial and Lgr5^{hi} cells: *Lgr5$^{EGFP,cre:ERT2}$* mice were sacrificed, excised intestines opened longitudinally, rinsed with cold saline, crypts isolated, single cell

suspensions prepared, cells sorted by FACs, and the 2-3% of cells with highest green fluorescence collected, as described (Li et al., 2019)

Bulk RNAseq analysis: construction of bulk RNAseq libraries, sequencing and data analysis were as described (Li et al., 2019).

Single cell RNAseq: Intestinal cells were isolated as above, re-suspended in antibody staining buffer, blocked with FcR Blocking Reagent (Miltenyi Biotec, 05244 T-30), washed and pelleted, then incubated for 20 minutes at 4^0C with, EpCAM-FITC (Miltenyi Biotec, Clone caa7-9G8, Cat No. 130-123-674) and CD45-PerCP (Miltenyi Biotec, Clone 30F11, Cat No. 130-123-879). Cells were sorted by FACs on a MoFlo instrument and Epcam positive, CD45 negative total or Bmi1+ epithelial cells collected.

Single cell RNAseq (scRNAseq) libraries were constructed by the Albert Einstein Genomics Core using the 3' kit protocols of 10X Genomics (San Francisco, CA) with approximately 10,000 single FACS collected cells from each mouse loaded onto a Chromium Chip B microfluidic apparatus (10X Genomics). Library quality was verified by size analysis (BioAnalyzer; Agilent, Santa Clara, CA) and after passing quality control assays, multiple libraries were mixed and sequenced by HiSeq PE150 or NovaSeq PE150 using pair-end sequencing, with a readout length of 150 bases (Novogene; Sacramento, California), and the data assigned to individual cells using the sample indexes.

For sequence alignment and subsequent analysis, output Illumina base call files were converted to FASTQ files (bcl2fastq), these from each mouse aligned to the mouse mm10 genome v1.2.0 and converted to count matrices (Cell Ranger software v3.0.2). Force-cell parameter was used, with 5000-8000 individual cells identified for each sample, and unique molecular identifiers (UMI) identified to remove PCR duplicates. Quality control and downstream analyses were done in R v4.0.2, using Seurat package v3.2.2 (Stuart et al., 2019). To discard doublets or dead cells, cells with gene counts <200 or >5000, or a mitochondrial gene ratio >20%, were filtered out. Cells from different samples were integrated using Seurat

FindIntegrationAnchors and IntegrateData functions, clusters identified from each of integrated data set using the Seurat FindClusters function. This calculates k-nearest neighbors according to Principle Component Analysis, constructs a shared nearest neighbor graph, and then optimizing a modularity function (Louvain algorithm) to determine cell clusters. Cell clusters were identified as cell intestinal cell types using established cell-type markers and cluster identification using Seurat FindMarkers function. Differential gene expression compared samples among experimental groups: initial criteria were an expression change of ≥1.5 fold with associated adjusted P-value of <0.01 in group comparison (Seurat FindMarkers function). Pathway analysis was performed on differentially expressed genes using clusterProfiler R package v3.16.1 and the KEGG pathway database (KEGG.db R package v3.2.4); gene set enrichment analysis (GSEA) used the fgsea R package v1.14.0, the MSigDB (v5.2) hallmark gene set and the KEGG pathway database. Pathways at $P < 0.05$ were considered statistically significant. Trajectory analysis used Monocle3 R package v0.2.3.3 (Trapnell et al., 2014) with cluster information and cell-type identifications migrated from Seurat using an in house computer script, the integrated dataset divided among different experimental conditions, and trajectories generated for each dietary or genetic condition.

RNAseq data have been deposited in the NCBI Gene Expression Omnibus (GEO) database: bulk RNAseq (Fig 1) - GSE186811; scRNAseq (Fig 4, *Ppargc1a* inactivation) - GSE188339; scRNAseq (Fig 5, rapid dietary crossover) - GSE188577; scRNAseq (Fig 6,7, Bmi1+ cells) - GSE188338.

***In situ* analyses:** Sections of Swiss rolls of mouse intestines fixed in 10% formalin were de-waxed and rehydrated. Reagents were from Advanced Cell Diagnostics (Newark, CA). Endogenous peroxidases were quenched and heat induced epitope retrieval done utilizing the RNAscope Multiplex Fluorescent Reagent Kit v2 (Cat. No. 323100) and the RNAscope Multiplex Fluorescent Assay v2 protocol followed. RNAscope target probes for *Bmi1* and *Ascl2* Cat No. 466021, 412211, respectively) were hybridized to sections and amplified using the

HybEZ Hybridization System (Cat No. 310010). Secondary TSA fluorophores from Akoya Biosciences were Opal 620 (channel 1, Cat No. FP1495001KT) and Opal 570 (channel 2, FP1488001KT), sections counterstained with Dapi and visualized using a Leica SP8 confocal microscope (20X magnification).

Immunohistochemistry: Swiss roll sections were de-waxed, rehydrated, endogenous peroxidases blocked (3% hydrogen peroxide in methanol) and heat induced epitope retrieval done with 10 mM Sodium citrate buffer (pH 6.0) for all antibodies. Tissues were incubated overnight at 4^0C with primary CD3 antibody (Novusbio, Littleton, CO, 1:10 dilution of NB600-1441). Protein block and secondary antibody for CD3 employed ImmPRESS-Alkaline Phosphatase Horse Anti-Rabbit IgG Polymer Kit-Alkaline Phosphatase (Vector Laboratories, Burlingame, CA, Cat No. MP-5401). F4/80 antibody (1:200, Cell Signaling, Denvers, MA, Cat No. 70076, Cell Signaling, Denvers, MA) was incubated on tissue overnight at 4^0C. Secondary antibody was SignalStain® Boost IHC Detection Reagent (HRP, Rabbit, Cell Signaling, Cat No. 8114). Counterstaining was with hematoxylin and visualization by bright field microscopy, or a CY5 filter for CD3.

Electron Microscopy: Samples were fixed with 2.5% glutaraldehyde, 2% paraformaldehyde in 0.1 M sodium cacodylate buffer, post-fixed with 1% osmium tetroxide followed by 2% uranyl acetate, dehydrated through a graded ethanol series and embedded in LX112 resin (LADD Research Industries, Burlington VT). Ultrathin sections were cut on a Leica Ultracut UC7, stained with uranyl acetate followed by lead citrate and viewed on a JEOL 1400 Plus transmission electron microscope at 120kv. Images were captured at a magnification of 800X, and at 5000X for quantitative measurements of mitochondrial size and cristae density.

Mitochondrial membrane potential: Crypts, isolated as reported, were dispersed into single-cell suspensions, and cells incubated with MitoTracker™ Red FM (Invitrogen, Cat # M22425, 25nM) for 20 min at 37 °C. Zombie NIR (Invitrogen, Cat # L10119) was added at the end of the

incubation to mark dead cells. Flow cytometry used a Cytek Aurora Instrument (Cytek Biosciences). Data were analyzed using Flowjo 10 software (Treestar Inc.).

Statistical Analysis of Ascl2 expression in Stem2: Fig 6G of the manuscript shows higher expression of *Ascl2* for a subset of cells in Stem2 for NWD1 mice longer term after Tam injection. The statistical significance of this minor cell population was determined in comparison to the other 3 mouse groups. A likelihood ratio test was significant (*P=0.01*, by a negative binomial regression-negative binomial mixed effect model, with regression and fit using R functions glm.nb and glmer.nb, respectively (Bates et al., 2015), assuming each cell as independent, and number of *Ascl2* reads for each cell as response). Post-hoc analysis by a similar negative binomial regression showed NWD1-LT differed significantly from the other 3 groups in *Ascl2* expression (*P=0.002*). Finally, potential that the difference between NWD1-LT and the other groups was random was tested using a negative binomial mixed effect model with mice per dietary group treated as random effects; the likelihood ratio test was *P = 0.11*, indicating the alternate hypothesis that effects were random is false.

Acknowledgements: Supported in part by R01CA229216, R01CA214625, R01CA222358 and P30CA013330 from the NCI, NIH, USPHS.

References:

Aslam, M. N., Paruchuri, T., Bhagavathula, N., and Varani, J. (2010). A mineral-rich red algae extract inhibits polyp formation and inflammation in the gastrointestinal tract of mice on a high-fat diet. Integr Cancer Ther *9*, 93-99.

Augenlicht, L. H. (2017a). Environmental Impact on Intestinal Stem Cell Functions in Mucosal Homeostasis and Tumorigenesis. J Cell Biochem *118*, 943-952.

Augenlicht, L. H. (2017b). Environmental Impact on Intestinal Stem Cell Functions in Mucosal Homeostasis and Tumorigenesis. Journal of Cellular Biochemistry *118*, 943-952.

Augenlicht, L. H., Taylor, J., Anderson, L., and Lipkin, M. (1991). Patterns of gene expression that characterize the colonic mucosa in patients at genetic risk for colonic cancer. ProcNatlAcadSciUSA *88*, 3286-3289.

Bardella, C., Pollard, P. J., and Tomlinson, I. (2011). SDH mutations in cancer. Biochim Biophys Acta *1807*, 1432-1443.

Bastias-Perez, M., Serra, D., and Herrero, L. (2020). Dietary Options for Rodents in the Study of Obesity. Nutrients *12*.

Bastie, C., Gaffney-Stomberg, E., Ting-Wen, L., Dhima, E., Pessin, J., and Augenlicht, L. (2012). Dietary cholecalcifero and calcium levels in a western-style defined rodent diet alter energy metabolism and inflammatory response in mice. J Nutrition *142*, 859-865.

Beswick, E. J., and Reyes, V. E. (2009). CD74 in antigen presentation, inflammation, and cancers of the gastrointestinal tract. World J Gastroenterol *15*, 2855-2861.

Beyaz, S., Chung, C., Mou, H., Bauer-Rowe, K. E., Xifaras, M. E., Ergin, I., Dohnalova, L., Biton, M., Shekhar, K., Eskiocak, O.*, et al.* (2021). Dietary suppression of MHC class II expression in intestinal epithelial cells enhances intestinal tumorigenesis. Cell Stem Cell *28*, 1922-1935 e1925.

Biton, M., Haber, A. L., Rogel, N., Burgin, G., Beyaz, S., Schnell, A., Ashenberg, O., Su, C. W., Smillie, C., Shekhar, K.*, et al.* (2018). T Helper Cell Cytokines Modulate Intestinal Stem Cell Renewal and Differentiation. Cell *175*, 1307-1320 e1322.

Breedveld, A., and van Egmond, M. (2019). IgA and FcalphaRI: Pathological Roles and Therapeutic Opportunities. Front Immunol *10*, 553.

Chen, L., Vasoya, R. P., Toke, N. H., Parthasarathy, A., Luo, S., Chiles, E., Flores, J., Gao, N., Bonder, E. M., Su, X., and Verzi, M. P. (2020). HNF4 Regulates Fatty Acid Oxidation and Is Required for Renewal of Intestinal Stem Cells in Mice. Gastroenterology *158*, 985-999 e989.

Choi, J., Rakhilin, N., Gadamsetty, P., Joe, D. J., Tabrizian, T., Lipkin, S. M., Huffman, D. M., Shen, X., and Nishimura, N. (2018). Intestinal crypts recover rapidly from focal damage with coordinated motion of stem cells that is impaired by aging. Scientific reports *8*, 10989.

Collins, T., Korman, A. J., Wake, C. T., Boss, J. M., Kappes, D. J., Fiers, W., Ault, K. A., Gimbrone, M. A., Jr., Strominger, J. L., and Pober, J. S. (1984). Immune interferon activates multiple class II major histocompatibility complex genes and the associated invariant chain gene in human endothelial cells and dermal fibroblasts. Proc Natl Acad Sci U S A *81*, 4917-4921.

D'Errico, I., Salvatore, L., Murzilli, S., Lo Sasso, G., Latorre, D., Martelli, N., Egorova, A. V., Polishuck, R., Madeyski-Bengtson, K., Lelliott, C.*, et al.* (2011). Peroxisome proliferator-activated receptor-gamma coactivator 1-alpha (PGC1alpha) is a metabolic regulator of intestinal epithelial cell fate. Proc Natl Acad Sci U S A *108*, 6603-6608.

Davies, K. J. (2016). Adaptive homeostasis. Molecular aspects of medicine *49*, 1-7.

de Jong, Y. P., Abadia-Molina, A. C., Satoskar, A. R., Clarke, K., Rietdijk, S. T., Faubion, W. A., Mizoguchi, E., Metz, C. N., Alsahli, M., ten Hove, T.*, et al.* (2001). Development of chronic colitis is dependent on the cytokine MIF. Nat Immunol *2*, 1061-1066.

Demay, M. B., MacDonald, P. N., Skorija, K., Dowd, D. R., Cianferotti, L., and Cox, M. (2007). Role of the vitamin D receptor in hair follicle biology. J Steroid Biochem Mol Biol *103*, 344-346.

Gold, D. V., Stein, R., Burton, J., and Goldenberg, D. M. (2010). Enhanced expression of CD74 in gastrointestinal cancers and benign tissues. Int J Clin Exp Pathol *4*, 1-12.

Gonzales, K. A. U., Polak, L., Matos, I., Tierney, M. T., Gola, A., Wong, E., Infarinato, N. R., Nikolova, M., Luo, S., Liu, S.*, et al.* (2021). Stem cells expand potency and alter tissue fitness by accumulating diverse epigenetic memories. Science *374*, eabh2444.

Hodder, M. C., Flanagan, D. J., and Sansom, O. J. (2018). Intestinal Stem Cell Dynamics: A Story of Mice and Humans. Cell Stem Cell *22*, 785-787.

Ishigami, S., Natsugoe, S., Tokuda, K., Nakajo, A., Iwashige, H., Aridome, K., Hokita, S., and Aikou, T. (2001). Invariant chain expression in gastric cancer. Cancer Lett *168*, 87-91.

Ito, K., Carracedo, A., Weiss, D., Arai, F., Ala, U., Avigan, D. E., Schafer, Z. T., Evans, R. M., Suda, T., Lee, C. H., and Pandolfi, P. P. (2012). A PML-PPAR-delta pathway for fatty acid oxidation regulates hematopoietic stem cell maintenance. Nat Med *18*, 1350-1358.

Iwata, R., Casimir, P., and Vanderhaeghen, P. (2020). Mitochondrial dynamics in postmitotic cells regulate neurogenesis. Science *369*, 858-862.

Jiang, Z., Xu, M., Savas, L., LeClair, P., and Banner, B. F. (1999). Invariant chain expression in colon neoplasms. Virchows Arch *435*, 32-36.

Keum, N., and Giovannucci, E. (2019). Global burden of colorectal cancer: emerging trends, risk factors and prevention strategies. Nat Rev Gastroenterol Hepatol *16*, 713-732.

Khoa, L. T. P., Tsan, Y. C., Mao, F., Kremer, D. M., Sajjakulnukit, P., Zhang, L., Zhou, B., Tong, X., Bhanu, N. V., Choudhary, C.*, et al.* (2020). Histone Acetyltransferase MOF Blocks Acquisition of Quiescence in Ground-State ESCs through Activating Fatty Acid Oxidation. Cell Stem Cell *27*, 441-458 e410.

Koehler, C. L., Perkins, G. A., Ellisman, M. H., and Jones, D. L. (2017). Pink1 and Parkin regulate Drosophila intestinal stem cell proliferation during stress and aging. J Cell Biol.

Lawrance, I. C., Fiocchi, C., and Chakravarti, S. (2001). Ulcerative colitis and Crohn's disease: distinctive gene expression profiles and novel susceptibility candidate genes. Hum Mol Genet *10*, 445-456.

Li, W., Peregrina, K., Houston, M., and Augenlicht, L. H. (2019a). Vitamin D and the nutritional environment in functions of intestinal stem cells: Implications for tumorigenesis and prevention. J Steroid Biochem Mol Biol *198*, 105556.

Li, W., Zimmerman, S., Peregrina, K., Houston, M., Mayoral, J., Zhang, J., Maqbool, S. B., Zhang, Z., Cai, Y., Ye, Q., and Augenlicht, L. (2019b). The nutritional environment determines which and how intestinal stem cells contribute to homeostasis and tumorigenesis. Carcinogenesis *40*, 937-946.

Lipkin, M., Blattner, W. E., Fraumeni, J. F., Lynch, H. T., Deschner, E., and Winawer, S. (1983). Tritiated thymidine (0p,0h)labeling distribution as a marker for hereditary predisposition to colon cancer. Cancer Res *43*, 1899-1904.

Lipkin, M., Friedman, E., Winawer, S. J., and Newmark, H. (1989). Colonic epithelial cell proliferation in responders and nonresponders to supplemental dietary calcium. Cancer Res *49*, 248-254.

Lipkin, M., and Newmark, H. (1985). Effect of added dietary calcium on colonic epithelial cell proliferation in subjects at high-risk for familial colon cancer. NEnglJMed *313*, 1381-1384.

Lipkin, M., Winawer, S. J., and Sherlock, P. (1981a). Early identification of individuals at increased risk for cancer of the large intestine. Part I: Definition of high risk populations. Clin Bull *11*, 13-21.

Lipkin, M., Winawer, S. J., and Sherlock, P. (1981b). Early identification of individuals at increased risk for cancer of the large intestine. Part II: Development of risk factor profiles. Clin Bull *11*, 66-74.

Lochhead, P., Chan, A. T., Nishihara, R., Fuchs, C. S., Beck, A. H., Giovannucci, E., and Ogino, S. (2015). Etiologic field effect: reappraisal of the field effect concept in cancer predisposition and progression. Mod Pathol *28*, 14-29.

Momburg, F., Koch, N., Moller, P., Moldenhauer, G., Butcher, G. W., and Hammerling, G. J. (1986). Differential expression of Ia and Ia-associated invariant chain in mouse tissues after in vivo treatment with IFN-gamma. J Immunol *136*, 940-948.

Moor, A. E., Harnik, Y., Ben-Moshe, S., Massasa, E. E., Rozenberg, M., Eilam, R., Bahar Halpern, K., and Itzkovitz, S. (2018). Spatial Reconstruction of Single Enterocytes Uncovers Broad Zonation along the Intestinal Villus Axis. Cell *175*, 1156-1167 e1115.

Munoz, J., Stange, D. E., Schepers, A. G., van de Wetering, M., Koo, B. K., Itzkovitz, S., Volckmann, R., Kung, K. S., Koster, J., Radulescu, S.*, et al.* (2012). The Lgr5 intestinal stem cell signature: robust expression of proposed quiescent '+4' cell markers. EMBO J *31*, 3079-3091.

Murata, K., Jadhav, U., Madha, S., van Es, J., Dean, J., Cavazza, A., Wucherpfennig, K., Michor, F., Clevers, H., and Shivdasani, R. A. (2020). Ascl2-Dependent Cell Dedifferentiation Drives Regeneration of Ablated Intestinal Stem Cells. Cell Stem Cell *26*, 377-390 e376.

Newmark, H. L., Lipkin, M., and Maheshwari, N. (1990). Colonic hyperplasia and hyperproliferation induced by a nutritional stress diet with four components of westen-style diet. J Nat Cancer Inst *82*, 491-496.

Newmark, H. L., Lipkin, M., and Maheshwari, N. (1991). Colonic hyperproliferation induced in rats and mice by nutritional-stress diets containing four components of a human western-style diet (series 2). Am J Clin Nutr *54*, 209S-214S.

Newmark, H. L., Yang, K., Kurihara, N., Fan, K., Augenlicht, L. H., and Lipkin, M. (2009). Western-style diet-induced colonic tumors and their modulation by calcium and vitamin D in C57Bl/6 mice: a preclinical model for human sporadic colon cancer. Carcinogenesis *30*, 88-92.

Newmark, H. L., Yang, K., Lipkin, M., Kopelovich, L., Liu, Y., Fan, K., and Shinozaki, H. (2001). A western-style diet induces benign and malignant neoplasms in the colon of normal C57Bl//6 mice. Carcinogenesis *22*, 1871-1875.

Nicholson, A. M., Olpe, C., Hoyle, A., Thorsen, A. S., Rus, T., Colombe, M., Brunton-Sim, R., Kemp, R., Marks, K., Quirke, P.*, et al.* (2018). Fixation and Spread of Somatic Mutations in Adult Human Colonic Epithelium. Cell Stem Cell *22*, 909-918 e908.

Parikh, K., Antanaviciute, A., Fawkner-Corbett, D., Jagielowicz, M., Aulicino, A., Lagerholm, C., Davis, S., Kinchen, J., Chen, H. H., Alham, N. K.*, et al.* (2019). Colonic epithelial cell diversity in health and inflammatory bowel disease. Nature *567*, 49-55.

Peregrina, K., Houston, M., Daroqui, C., Dhima, E., Sellers, R. S., and Augenlicht, L. H. (2015). Vitamin D is a determinant of mouse intestinal Lgr5 stem cell function. Carcinogenesis *36*, 25-31.

Puigserver, P., and Spiegelman, B. M. (2003). Peroxisome proliferator-activated receptor-gamma coactivator 1 alpha (PGC-1 alpha): transcriptional coactivator and metabolic regulator. Endocr Rev *24*, 78-90.

Rodriguez-Colman, M. J., Schewe, M., Meerlo, M., Stigter, E., Gerrits, J., Pras-Raves, M., Sacchetti, A., Hornsveld, M., Oost, K. C., Snippert, H. J.*, et al.* (2017). Interplay between metabolic identities in the intestinal crypt supports stem cell function. Nature *543*, 424-427.

Schroder, B. (2016). The multifaceted roles of the invariant chain CD74--More than just a chaperone. Biochim Biophys Acta *1863*, 1269-1281.

Schuijers, J., Junker, J. P., Mokry, M., Hatzis, P., Koo, B. K., Sasselli, V., van der Flier, L. G., Cuppen, E., van Oudenaarden, A., and Clevers, H. (2015). Ascl2 acts as an R-spondin/Wnt-responsive switch to control stemness in intestinal crypts. Cell Stem Cell *16*, 158-170.

Shivdasani, R. A. (2021). Race to the bottom: Darwinian competition in early intestinal tumorigenesis. Cell Stem Cell *28*, 1340-1342.

Shivdasani, R. A., Clevers, H., and de Sauvage, F. J. (2021). Tissue regeneration: Reserve or reverse? Science *371*, 784-786.

Speakman, J. R. (2019). Use of high-fat diets to study rodent obesity as a model of human obesity. Int J Obes (Lond) *43*, 1491-1492.

Stauber, J., Greally, J. M., and Steidl, U. (2021). Preleukemic and leukemic evolution at the stem cell level. Blood *137*, 1013-1018.

Steck, S. E., and Murphy, E. A. (2020). Dietary patterns and cancer risk. Nat Rev Cancer *20*, 125-138.

Suzuki, Y., Landowski, C. P., and Hediger, M. A. (2008). Mechanisms and regulation of epithelial Ca2+ absorption in health and disease. Annu Rev Physiol *70*, 257-271.

Tamori, Y., Tan, X., Nakagawa, K., Takai, E., Akagi, J., Kageshita, T., Egami, H., and Ogawa, M. (2005). Clinical significance of MHC class II-associated invariant chain expression in human gastric carcinoma. Oncol Rep *14*, 873-877.

Volc-Platzer, B., Majdic, O., Knapp, W., Wolff, K., Hinterberger, W., Lechner, K., and Stingl, G. (1984). Evidence of HLA-DR antigen biosynthesis by human keratinocytes in disease. J Exp Med *159*, 1784-1789.

Wang, D., Peregrina, K., Dhima, E., Lin, E. Y., Mariadason, J. M., and Augenlicht, L. H. (2011). Paneth cell marker expression in intestinal villi and colon crypts characterizes dietary induced risk for mouse sporadic intestinal cancer. Proc Natl Acad Sci U S A *108*, 10272-10277.

Wei, E. K., Colditz, G. A., Giovannucci, E. L., Wu, K., Glynn, R. J., Fuchs, C. S., Stampfer, M., Willett, W., Ogino, S., and Rosner, B. (2017). A Comprehensive Model of Colorectal Cancer by Risk Factor Status and Subsite Using Data From the Nurses' Health Study. Am J Epidemiol.

Wosen, J. E., Mukhopadhyay, D., Macaubas, C., and Mellins, E. D. (2018). Epithelial MHC Class II Expression and Its Role in Antigen Presentation in the Gastrointestinal and Respiratory Tracts. Front Immunol *9*, 2144.

Wu, Z., Puigserver, P., Andersson, U., Zhang, C., Adelmant, G., Mootha, V., Troy, A., Cinti, S., Lowell, B., Scarpulla, R. C., and Spiegelman, B. M. (1999). Mechanisms controlling mitochondrial biogenesis and respiration through the thermogenic coactivator PGC-1. Cell *98*, 115-124.

Xia, H. H., Lam, S. K., Chan, A. O., Lin, M. C., Kung, H. F., Ogura, K., Berg, D. E., and Wong, B. C. (2005). Macrophage migration inhibitory factor stimulated by Helicobacter pylori increases proliferation of gastric epithelial cells. World J Gastroenterol *11*, 1946-1950.

Yang, K., Edelmann, W., Fan, K., Lau, K., Leung, D., Newmark, H., Kucherlapati, R., and Lipkin, M. (1998). Dietary modulation of carcinoma development in a mouse model for human familial polyposis. Cancer Res *58*, 5713-5717.

Yang, K., Kurihara, N., Fan, K., Newmark, H., Rigas, B., Bancroft, L., Corner, G., Livote, E., Lesser, M., Edelmann, W.*, et al.* (2008a). Dietary induction of colonic tumors in a mouse model of sporadic colon cancer. Cancer Res *68*, 7803-7810.

Yang, K., Popova, N., Yang, W., Lozonschi, I., Tadesse, S., Kent, S., Bancroft, L., Matise, I., Cormier, R., Scherer, S.*, et al.* (2008b). Interaction of Muc2 and Apc on Wnt signaling and in intestinal tumorigenesis: potential role of chronic inflammation. Cancer Res *68*, 7313-7322.

Yang, W., Bancroft,L., Nicholas, C., Lozonschi, I., Augenlicht, L.H. (2003). Targeted inactivation of p27kip1 is sufficient for large and small intestinal tumorigenesis in the mouse, which can be augmented by a western-style high-risk diet. Cancer Res *63*, 4990-4996.

Yang, W. C., Mathew, J., Velcich, A., Edelmann, W., Kucherlapati, R., Lipkin, M., Yang, K., and Augenlicht, L. H. (2001). Targeted inactivation of the p21 WAF1/cip1 gene enhances Apc initiated tumor formation and the tumor promoting activity of a Western-style high risk diet by altering cell maturation in the intestinal mucosa. Cancer Res *61*, 565-569.

Zhang, D., Wang, W., Xiang, B., Li, N., Huang, S., Zhou, W., Sun, Y., Wang, X., Ma, J., Li, G.*, et al.* (2013). Reduced succinate dehydrogenase B expression is associated with growth and de-differentiation of colorectal cancer cells. Tumour Biol *34*, 2337-2347.

Figure Legends:

Figure 1: Bulk RNAseq analysis of Lgr5^{hi} cells: A, *Lgr5$^{EGFP.cre:ER}$* mice fed AIN76A or NWD1 for 3 or 12 months from weaning, or NWD1 for 3 months then switched to AIN76A for 9 months (cross-over); **B,** Expression ratio at 12 vs 3 months of 504 genes of an Lgr5^{hi} stem cell signature (Munoz et al., 2012), for AIN76A or NWD1 fed mice. **C,** percent of the 504 genes with expression ratio greater or less than 1 at 12 vs 3 month; **D,** number Lgr^{hi} cell sequences up or down-regulated for stem cell signature genes, or ~8,000 expressed genes in the experimental arms; **E,** pathways upregulated (green) or **F**, downregulated (red), by GSEA analysis, in Lgr5^{hi} cells after feeding NWD1 for 3 or 12 months, and in diet reversal. For each pathway, columns are NES, P-value, and FDR (false discovery rate).

Figure 2: Dietary Impact on Oxphos genes in Lgr5^{hi} cells: A, Expression ratio of oxphos pathway genes in mice fed NWD1 vs AIN76A for 3 months (Fig 1A) and from interrogating an independent RNAseq data set (Li et al., 2019b); **B,** down-regulated expression of Oxphos genes in each complex of the mitochondrial electron transport chain; **C**, expression ratio at 3 months of feeding NWD1 vs AIN76A in each independent data set, or **D,** at 12 months, mean decrease, and number and % of genes reversed by dietary cross-over.

Figure 3: Dietary Impact on *Ppargc1a* and mitochondria: Lgr5^{hi} cell *Ppargc1a* expression from: **A**, **B,** bulk RNAseq data bases of Fig 1A; **C**, interrogation of a previously reported bulk-RNA seq data bases at 3 months of feeding; **D,** immunohistochemical detection of Pgc1 in crypts of mice fed diets for 3 months; **E**, quantitation of Pgc1a immunohistochemistry by position along the crypt-villus axis; **F**, *Ppargc1a* expression in Lgr5^{hi} and Bmi1+ cells from scRNAseq analysis of mice fed different diets for 3 months (Fig 6); **G**, crypt base cell electron microscopy in mice fed different diets, arrows indicate cristae (800X); **H**, quantitation of mitochondrial cristae density in CBC, Paneth, and villus cells evaluated at 5000X magnification; **I,J**,**K** FACs analysis Lgr5^{hi} cell number, and **L**, Mitotracker staining, of mice fed diets for 3 months. *(*P<0.05, **0.01, ***0.001*).

Figure 4: Genetic inactivation of *Pprargc1a* in Lgr5 cells: A, suppressed lineage tracing from Lgr5^{hi} cells by homozygous inactivation of *Ppargc1a* in *Lgr5$^{cre:er-GFP}$, Ppargc1a$^{F/F\ or\ F/+}$, Rosa26^{tom}* mice fed control diet, 3 days post a single Tam injection, and **B**, quantitation; **C,** trajectory analysis of cells analyzed by scRNAseq of total intestinal epithelial cells from wild-type mice or 3 days after hetero- or homozygous *Ppargc1a* inactivation: yellow arrow, Stem cell cluster, *N=3* for each group; **D,E,** cell type distribution at branch point "a" in trajectory analysis (red arrow, Fig4C); **F,** altered pathways and most significantly altered genes at branch a; **G,H,** analysis of cell type distribution at branch point "b" " (red arrow, Fig4C); **J** altered pathways and most significantly altered genes at branch b;

Figure 5: Rapid reprogramming of cells by dietary shift: A, mice fed AIN76A for 3 months (Arm1), switched to NWD1 for 4 days (Arm 2), or then switched back to AIN76A for 4 days, total Epcam+, CD45neg epithelial cells FACs isolated and analyzed by scRNAseq; **B, C,** pathways altered by rapid dietary shifts; **D**, for the stem cell cluster, genes encoding TCA cycle enzymes repressed by 4d switch to NWD1 from AIN76A, and then reversed when mice were switched back to AIN76A for 4d; **E**, trajectory analysis of cells identified from the scRNAseq analyses:

yellow arrow, Stem cell cluster, *N=3* each group; **F,G.** cell type distribution at branch point "a" (red arrow in trajectory analysis (Fig. 5E); **H,** altered pathways and most significantly altered genes in cells at branch a; **I**,**J**, cell type distribution at branch point "b" (red arrow, in trajectory analysis (Fig. 5E); **K,** altered pathways and most significantly altered genes in cells at branch point b.

Figure 6: scRNAseq of Bmi1+ intestinal epithelial cells in response to diet: A, Rosa26^{tom} marked Epcam+, CD45neg epithelial cells FACs isolated from *Bm1$^{cre:er}$, Rosa26^{tom}* mice fed AIN76A or NWD1 for 3 months, either 3 or 66-70 days after TAM injection to activate the Rosa marker (shorter, longer term, respectively) and analyzed by scRNAseq (*N-2 for each group);* **B,** intestinal epithelial cell type/lineage distribution by diet and time post tam marking of cells**; C,** cell cluster trajectory analysis as a function of diet and time post marking by tamoxifen injection; **D, E** *Ascl2* expressing cells among clusters: blue arrow, stem and progenitor cells; yellow arrows, goblet and enteroendocrine cells; **F,G**, Expression of *Ascl2* per cell in Stem1, 2, Replicating and Dividing cells: red arrow in G denotes a Stem 2 cell population that expressed *Ascl2* at a higher level; **H,** *Ascl2* and *Bmi1* expression by *in situ* hybridization in mice fed diets for 3 months: white dotted line demarks the crypt base; **I,** cell type distribution at branch points "1" and "2" (red arrows, trajectory analysis (Fig. 6C); **J**, *Ascl2* expression per cell at branch point 2

Figure 7: NWD1 expansion of an enterocyte population: A, number of differentially expressed genes (>50% *and P=0.01*) in Bmi1 cell clusters of Fig S5B/Fig S6C; **B,** Heat map of genes differentially expressed by diet in EC7 cells; **C,** EC7 cell pathways enriched by GSEA analysis as a function of diet and time post marking of Bmi1+ cells; **D**, distribution of cells expressing CD74, and **E**, CD74 expression per cell, in cell types/lineages as a function of diet and time post marking of Bmi1+ cells; **F**,I GSEA analysis of Fatty acid metabolism pathway for

all clusters by rapid dietary shift (Fig 5A); **G**, TrpV6 expression in each cell of Bmi1+ cell clusters in mice fed AIN76A or NWD1 (Fig 6A).

Figures
Choi et al.

Fig. 1

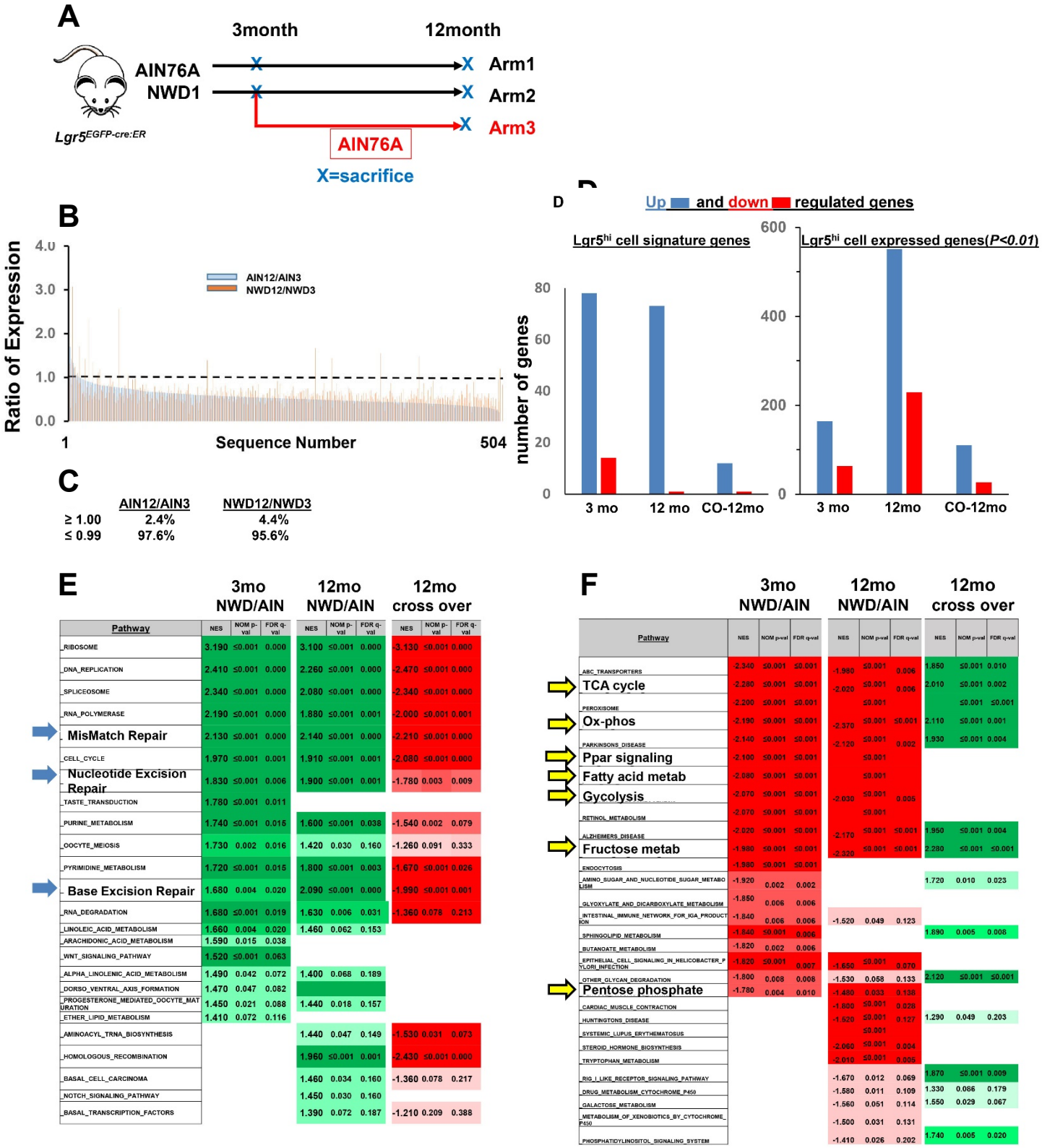
A
3month
12month
AIN76A
NWD1
Arm1
Arm2
Arm3
Lgr5EGFP-cre:ER
AIN76A
X=sacrifice
B
Ratio of Expression
4.0
3.0
2.0
1.0
0.0
AIN12/AIN3
NWD12/NWD3
1
Sequence Number
504
C
AIN12/AIN3
NWD12/NWD3
≥ 1.00 2.4% 4.4%
≤ 0.99 97.6% 95.6%
D
Up and down regulated genes
Lgr5hi cell signature genes
Lgr5hi cell expressed genes(P<0.01)
number of genes
3 mo
12 mo
CO-12mo
3 mo
12mo
CO-12mo
E
3mo NWD/AIN
12mo NWD/AIN
12mo cross over
Pathway
NES NOM p-val FDR q-val
_RIBOSOME 3.190 ≤0.001 0.000 3.100 ≤0.001 0.000 -3.130 ≤0.001 0.000
_DNA_REPLICATION 2.410 ≤0.001 0.000 2.260 ≤0.001 0.000 -2.470 ≤0.001 0.000
_SPLICEOSOME 2.340 ≤0.001 0.000 2.080 ≤0.001 0.000 -2.340 ≤0.001 0.000
_RNA_POLYMERASE 2.190 ≤0.001 0.000 1.880 ≤0.001 0.001 -2.000 ≤0.001 0.001
MisMatch Repair 2.130 ≤0.001 0.000 2.140 ≤0.001 0.000 -2.210 ≤0.001 0.000
_CELL_CYCLE 1.970 ≤0.001 0.001 1.910 ≤0.001 0.001 -2.080 ≤0.001 0.000
Nucleotide Excision Repair 1.830 ≤0.001 0.006 1.900 ≤0.001 0.001 -1.780 0.003 0.009
_TASTE_TRANSDUCTION 1.780 ≤0.001 0.011
_PURINE_METABOLISM 1.740 ≤0.001 0.015 1.600 ≤0.001 0.038 -1.540 0.002 0.079
_OOCYTE_MEIOSIS 1.730 0.002 0.016 1.420 0.030 0.160 -1.260 0.091 0.333
_PYRIMIDINE_METABOLISM 1.720 ≤0.001 0.015 1.800 ≤0.001 0.003 -1.670 ≤0.001 0.026
Base Excision Repair 1.680 0.004 0.020 2.090 ≤0.001 0.000 -1.990 ≤0.001 0.001
_RNA_DEGRADATION 1.680 ≤0.001 0.019 1.630 0.006 0.031 -1.360 0.078 0.213
_LINOLEIC_ACID_METABOLISM 1.660 0.004 0.020 1.460 0.062 0.153
_ARACHIDONIC_ACID_METABOLISM 1.590 0.015 0.038
_WNT_SIGNALING_PATHWAY 1.520 ≤0.001 0.063
_ALPHA_LINOLENIC_ACID_METABOLISM 1.490 0.042 0.072 1.400 0.068 0.189
_DORSO_VENTRAL_AXIS_FORMATION 1.470 0.047 0.082
_PROGESTERONE_MEDIATED_OOCYTE_MATURATION 1.450 0.021 0.088 1.440 0.018 0.157
_ETHER_LIPID_METABOLISM 1.410 0.072 0.116
_AMINOACYL_TRNA_BIOSYNTHESIS 1.440 0.047 0.149 -1.530 0.031 0.073
_HOMOLOGOUS_RECOMBINATION 1.960 ≤0.001 0.001 -2.430 ≤0.001 0.000
_BASAL_CELL_CARCINOMA 1.460 0.034 0.160 -1.360 0.078 0.217
_NOTCH_SIGNALING_PATHWAY 1.450 0.030 0.160
_BASAL_TRANSCRIPTION_FACTORS 1.390 0.072 0.187 -1.210 0.209 0.388
F
3mo NWD/AIN
12mo NWD/AIN
12mo cross over
Pathway
NES NOM p-val FDR q-val
_ABC_TRANSPORTERS -2.340 ≤0.001 ≤0.001 -1.980 ≤0.001 0.006 1.850 ≤0.001 0.010
TCA cycle -2.280 ≤0.001 ≤0.001 -2.020 ≤0.001 0.006 2.010 ≤0.001 0.002
_PEROXISOME -2.200 ≤0.001 ≤0.001 ≤0.001 ≤0.001 ≤0.001
Ox-phos -2.190 ≤0.001 ≤0.001 -2.370 ≤0.001 ≤0.001 2.110 ≤0.001 0.001
_PARKINSONS_DISEASE -2.140 ≤0.001 ≤0.001 -2.120 ≤0.001 0.002 1.930 ≤0.001 0.004
Ppar signaling -2.100 ≤0.001 ≤0.001 ≤0.001
Fatty acid metab -2.080 ≤0.001 ≤0.001 ≤0.001
Gycolysis -2.070 ≤0.001 ≤0.001 -2.030 ≤0.001 0.005
_RETINOL_METABOLISM -2.070 ≤0.001 ≤0.001 ≤0.001
_ALZHEIMERS_DISEASE -2.020 ≤0.001 ≤0.001 -2.170 ≤0.001 ≤0.001 1.950 ≤0.001 0.004
Fructose metab -1.980 ≤0.001 ≤0.001 -2.320 ≤0.001 ≤0.001 2.280 ≤0.001 ≤0.001
_ENDOCYTOSIS -1.980 ≤0.001 ≤0.001
_AMINO_SUGAR_AND_NUCLEOTIDE_SUGAR_METABOLISM -1.920 0.002 0.002 1.720 0.010 0.023
_GLYOXYLATE_AND_DICARBOXYLATE_METABOLISM -1.850 0.006 0.006
_INTESTINAL_IMMUNE_NETWORK_FOR_IGA_PRODUCTION -1.840 0.006 0.006 -1.520 0.049 0.123
_SPHINGOLIPID_METABOLISM -1.840 ≤0.001 0.006 1.890 0.005 0.008
_BUTANOATE_METABOLISM -1.820 0.002 0.006
_EPITHELIAL_CELL_SIGNALING_IN_HELICOBACTER_PYLORI_INFECTION -1.820 ≤0.001 0.007 -1.650 ≤0.001 0.070
_OTHER_GLYCAN_DEGRADATION -1.800 0.008 0.008 -1.530 0.058 0.133 2.120 ≤0.001 ≤0.001
Pentose phosphate -1.780 0.004 0.010 -1.480 0.033 0.138
_CARDIAC_MUSCLE_CONTRACTION -1.800 ≤0.001 0.028
_HUNTINGTONS_DISEASE -1.520 ≤0.001 0.127 1.290 0.049 0.203
_SYSTEMIC_LUPUS_ERYTHEMATOSUS ≤0.001
_STEROID_HORMONE_BIOSYNTHESIS -2.060 ≤0.001 0.004
_TRYPTOPHAN_METABOLISM -2.010 ≤0.001 0.005
_RIG_I_LIKE_RECEPTOR_SIGNALING_PATHWAY -1.670 0.012 0.069 1.870 ≤0.001 0.009
_DRUG_METABOLISM_CYTOCHROME_P450 -1.580 0.011 0.109 1.330 0.086 0.179
_GALACTOSE_METABOLISM -1.560 0.051 0.114 1.550 0.029 0.067
_METABOLISM_OF_XENOBIOTICS_BY_CYTOCHROME_P450 -1.500 0.031 0.131
_PHOSPHATIDYLINOSITOL_SIGNALING_SYSTEM -1.410 0.026 0.202 1.740 0.005 0.020

Fig. 2

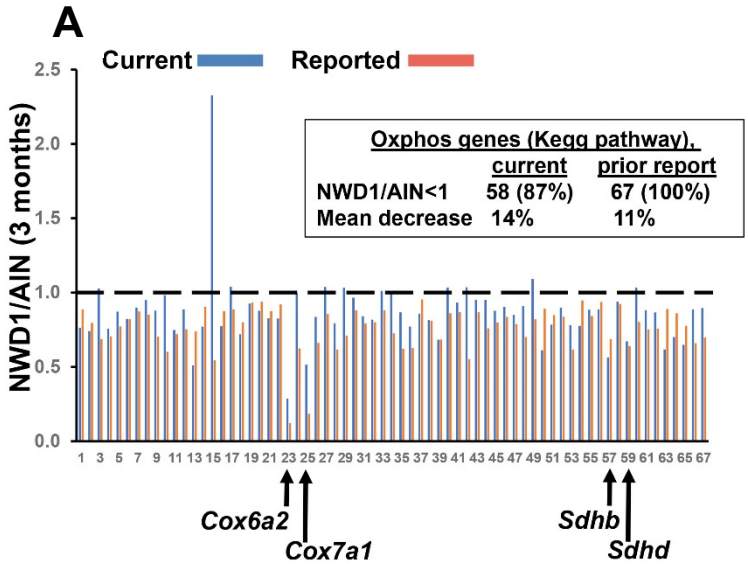

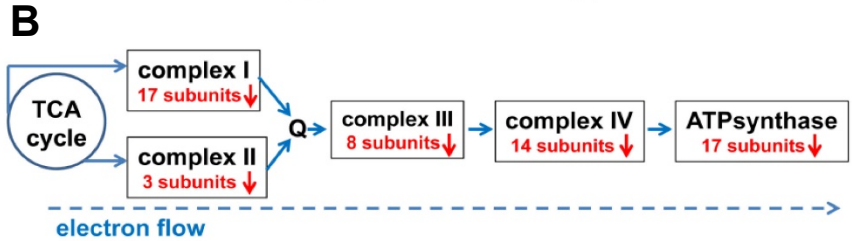

C

NWD1/AIN76A

	current	from prior data set
Cox6a2	0.29	0.12
Cox7a1	0.52	0.19
Sdhb	0.56	0.69
Sdhd	0.67	0.64

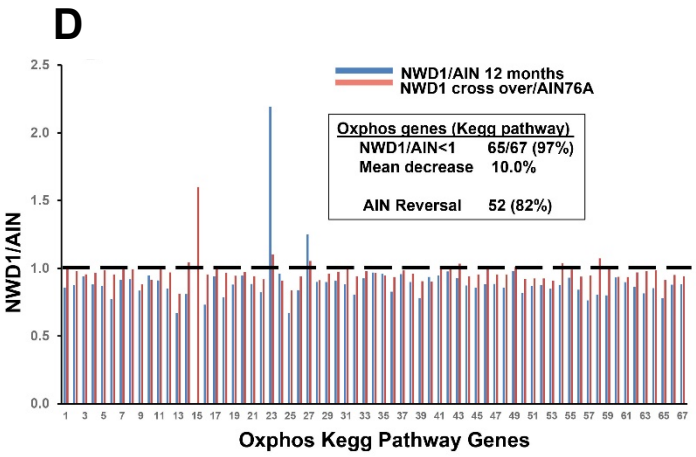

Fig. 3

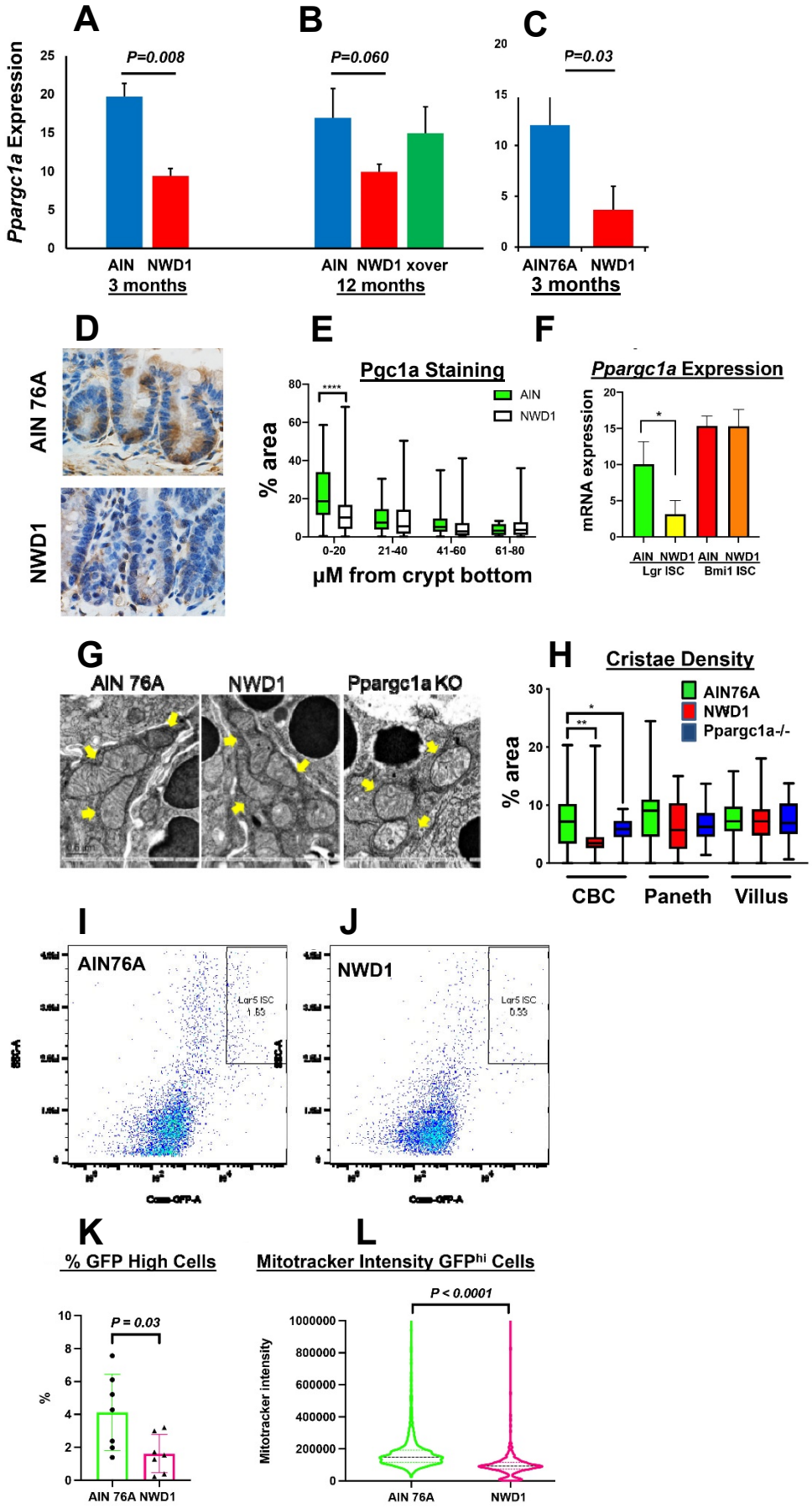
A
Ppargc1a Expression
P=0.008
AIN NWD1
3 months
B
P=0.060
AIN NWD1 xover
12 months
C
P=0.03
AIN76A NWD1
3 months
D
AIN 76A
NWD1
E
Pgc1a Staining
% area
AIN
NWD1
0-20
21-40
41-60
61-80
µM from crypt bottom
F
Ppargc1a Expression
mRNA expression
AIN NWD1 AIN NWD1
Lgr ISC Bmi1 ISC
G
AIN 76A
NWD1
Ppargc1a KO
H
Cristae Density
AIN76A
NWD1
Ppargc1a-/-
% area
CBC
Paneth
Villus
I
AIN76A
J
NWD1
K
% GFP High Cells
P = 0.03
%
AIN 76A NWD1
L
Mitotracker Intensity GFPhi Cells
P < 0.0001
Mitotracker intensity
AIN 76A
NWD1

Fig. 4

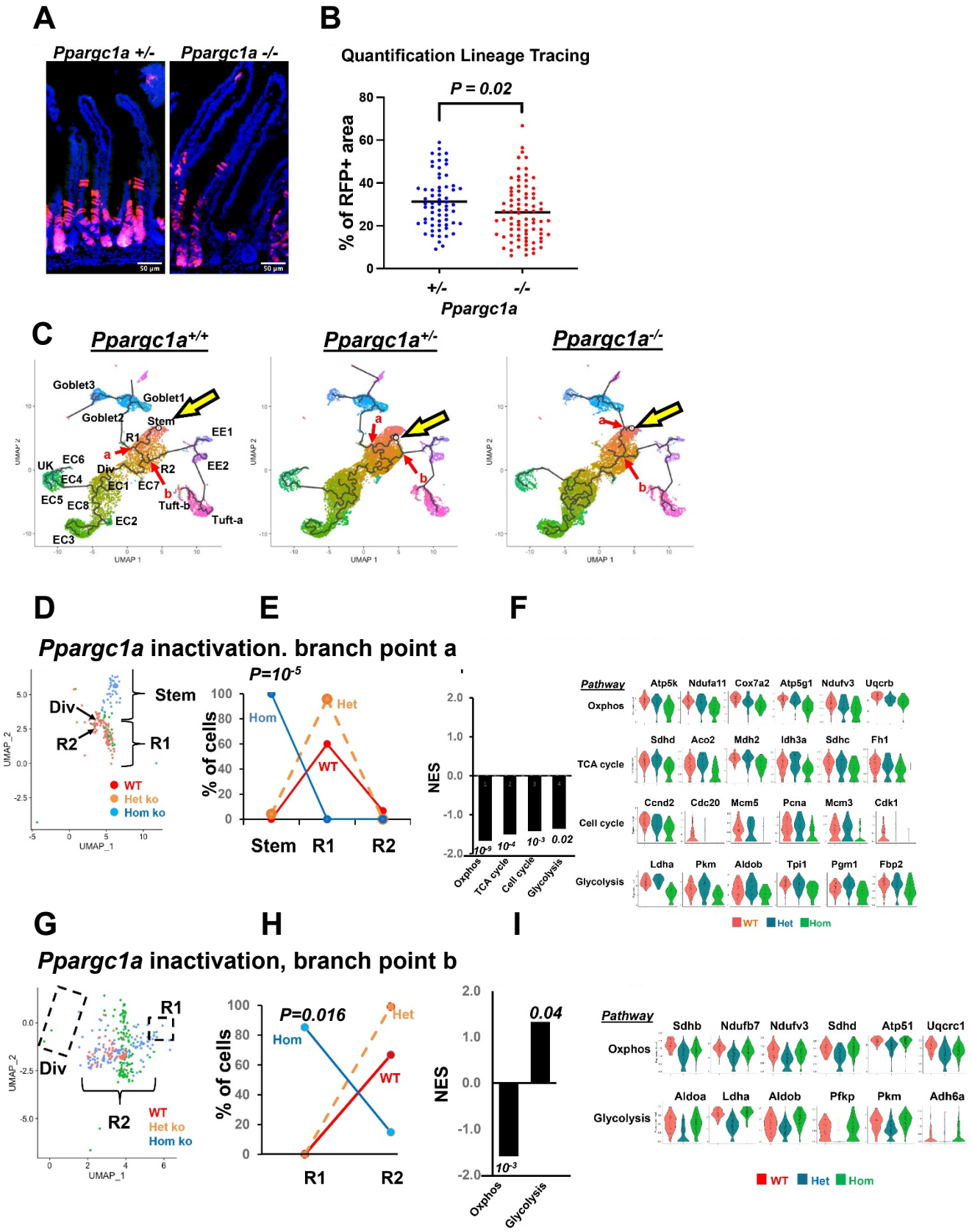
A
Ppargc1a +/-
Ppargc1a -/-
B
Quantification Lineage Tracing
P = 0.02
% of RFP+ area
+/-
-/-
Ppargc1a
C
Ppargc1a+/+
Ppargc1a+/-
Ppargc1a-/-
Goblet3
Goblet1
Goblet2
Stem
EE1
EE2
R1
R2
Div
UK
EC6
EC4
EC1
EC7
EC5
EC8
EC2
EC3
Tuft-b
Tuft-a
UMAP 1
UMAP 2
D
E
F
Ppargc1a inactivation. branch point a
Stem
R1
R2
WT
Het ko
Hom ko
UMAP_1
UMAP_2
P=10-5
Hom
Het
WT
% of cells
Stem
R1
R2
NES
Oxphos
TCA cycle
Cell cycle
Glycolysis
Pathway
Atp5k
Ndufa11
Cox7a2
Atp5g1
Ndufv3
Uqcrb
Sdhd
Aco2
Mdh2
Idh3a
Sdhc
Fh1
Ccnd2
Cdc20
Mcm5
Pcna
Mcm3
Cdk1
Ldha
Pkm
Aldob
Tpi1
Pgm1
Fbp2
WT
Het
Hom
G
H
I
Ppargc1a inactivation, branch point b
R1
Div
R2
WT
Het ko
Hom ko
UMAP_1
UMAP_2
P=0.016
Hom
Het
WT
% of cells
R1
R2
NES
0.04
Oxphos
Glycolysis
Pathway
Sdhb
Ndufb7
Ndufv3
Sdhd
Atp51
Uqcrc1
Aldoa
Ldha
Aldob
Pfkp
Pkm
Adh6a
WT
Het
Hom

Fig. 5

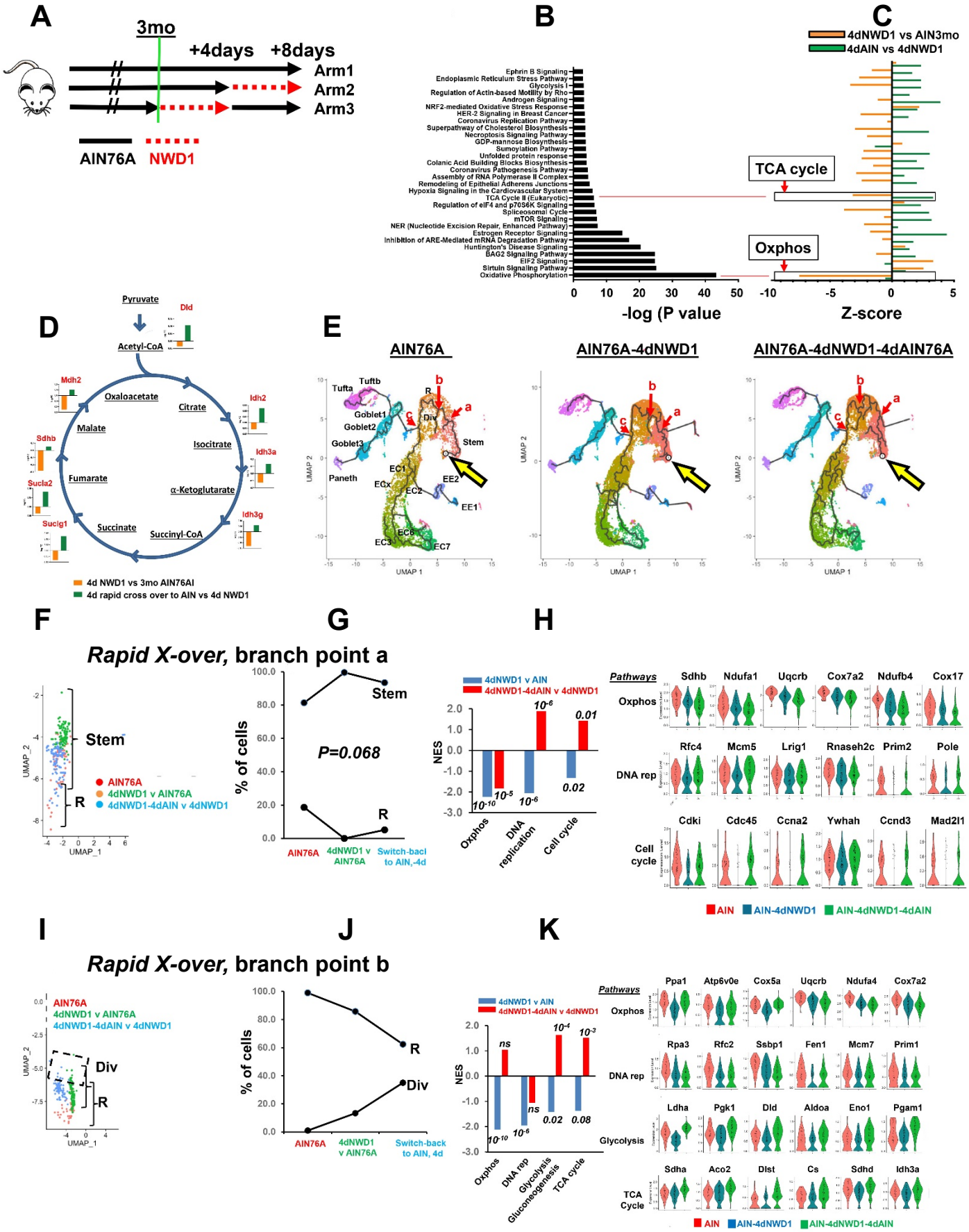
A
3mo
+4days
+8days
Arm1
Arm2
Arm3
AIN76A
NWD1
B
Ephrin B Signaling
Endoplasmic Reticulum Stress Pathway
Glycolysis I
Regulation of Actin-based Motility by Rho
Androgen Signaling
NRF2-mediated Oxidative Stress Response
HER-2 Signaling in Breast Cancer
Coronavirus Replication Pathway
Superpathway of Cholesterol Biosynthesis
Necroptosis Signaling Pathway
GDP-mannose Biosynthesis
Sumoylation Pathway
Unfolded protein response
Colanic Acid Building Blocks Biosynthesis
Coronavirus Pathogenesis Pathway
Assembly of RNA Polymerase II Complex
Remodeling of Epithelial Adherens Junctions
Hypoxia Signaling in the Cardiovascular System
TCA Cycle II (Eukaryotic)
Regulation of eIF4 and p70S6K Signaling
Spliceosomal Cycle
mTOR Signaling
NER (Nucleotide Excision Repair, Enhanced Pathway)
Estrogen Receptor Signaling
Inhibition of ARE-Mediated mRNA Degradation Pathway
Huntington's Disease Signaling
BAG2 Signaling Pathway
EIF2 Signaling
Sirtuin Signaling Pathway
Oxidative Phosphorylation
0 10 20 30 40 50
-log (P value
C
4dNWD1 vs AIN3mo
4dAIN vs 4dNWD1
TCA cycle
Oxphos
-10 -5 0 5
Z-score
D
Pyruvate
Dld
Acetyl-CoA
Oxaloacetate
Citrate
Isocitrate
α-Ketoglutarate
Succinyl-CoA
Succinate
Fumarate
Malate
Mdh2
Idh2
Idh3a
Idh3g
Sdhb
Sucla2
Suclg1
4d NWD1 vs 3mo AIN76AI
4d rapid cross over to AIN vs 4d NWD1
E
AIN76A
AIN76A-4dNWD1
AIN76A-4dNWD1-4dAIN76A
Tufta
Tuftb
Goblet1
Goblet2
Goblet3
Paneth
Stem
Div
EC1
EC2
ECx
EC3
EC6
EC7
EE1
EE2
UMAP 1
UMAP 2
F
Rapid X-over, branch point a
Stem
R
AIN76A
4dNWD1 v AIN76A
4dNWD1-4dAIN v 4dNWD1
UMAP_1
UMAP_2
G
% of cells
P=0.068
Stem
R
AIN76A
4dNWD1 v AIN76A
Switch-back to AIN, 4d
H
4dNWD1 v AIN
4dNWD1-4dAIN v 4dNWD1
NES
Oxphos
DNA replication
Cell cycle
Pathways
Sdhb Ndufa1 Uqcrb Cox7a2 Ndufb4 Cox17
Rfc4 Mcm5 Lrig1 Rnaseh2c Prim2 Pole
Cdki Cdc45 Ccna2 Ywhah Ccnd3 Mad2l1
AIN
AIN-4dNWD1
AIN-4dNWD1-4dAIN
I
Rapid X-over, branch point b
AIN76A
4dNWD1 v AIN76A
4dNWD1-4dAIN v 4dNWD1
Div
R
UMAP_1
UMAP_2
J
% of cells
R
Div
AIN76A
4dNWD1 v AIN76A
Switch-back to AIN, 4d
K
4dNWD1 v AIN
4dNWD1-4dAIN v 4dNWD1
NES
Oxphos
DNA rep
Glycolysis
Gluconeogenesis
TCA cycle
Pathways
Ppa1 Atp6v0e Cox5a Uqcrb Ndufa4 Cox7a2
Rpa3 Rfc2 Ssbp1 Fen1 Mcm7 Prim1
Ldha Pgk1 Dld Aldoa Eno1 Pgam1
Sdha Aco2 Dlst Cs Sdhd Idh3a
TCA Cycle
AIN
AIN-4dNWD1
AIN-4dNWD1-4dAIN

Fig. 6

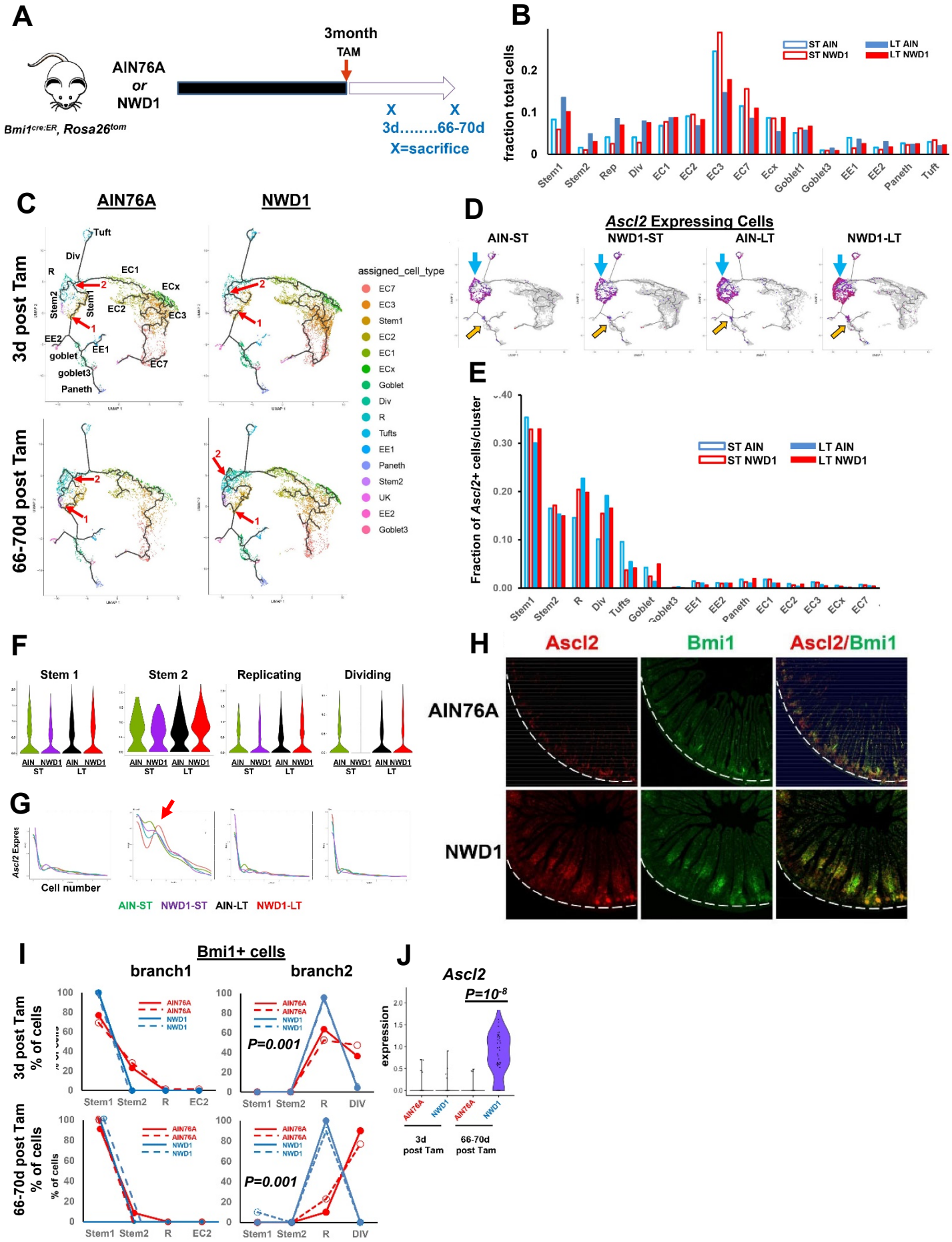
A
3month
TAM
AIN76A
or
NWD1
Bmi1cre:ER, Rosa26tom
X
X
3d.....66-70d
X=sacrifice
B
fraction total cells
ST AIN
ST NWD1
LT AIN
LT NWD1
Stem1
Stem2
Rep
Div
EC1
EC2
EC3
EC7
Ecx
Goblet1
Goblet3
EE1
EE2
Paneth
Tuft
C
AIN76A
NWD1
3d post Tam
66-70d post Tam
assigned_cell_type
EC7
EC3
Stem1
EC2
EC1
ECx
Goblet
Div
R
Tufts
EE1
Paneth
Stem2
UK
EE2
Goblet3
D
Ascl2 Expressing Cells
AIN-ST
NWD1-ST
AIN-LT
NWD1-LT
E
Fraction of Ascl2+ cells/cluster
ST AIN
ST NWD1
LT AIN
LT NWD1
F
Stem 1
Stem 2
Replicating
Dividing
AIN NWD1 AIN NWD1
ST LT
G
Ascl2 Expres
Cell number
AIN-ST
NWD1-ST
AIN-LT
NWD1-LT
H
Ascl2
Bmi1
Ascl2/Bmi1
AIN76A
NWD1
I
Bmi1+ cells
branch1
branch2
3d post Tam
% of cells
66-70d post Tam
% of cells
AIN76A
NWD1
P=0.001
P=0.001
Stem1
Stem2
R
EC2
DIV
J
Ascl2
P=10-8
expression
AIN76A
NWD1
3d
post Tam
66-70d
post Tam

Fig. 7

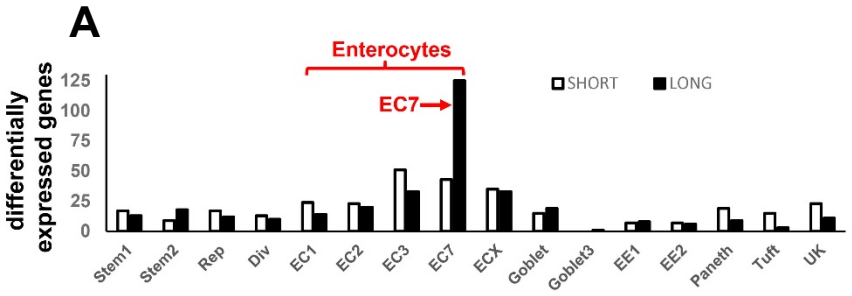

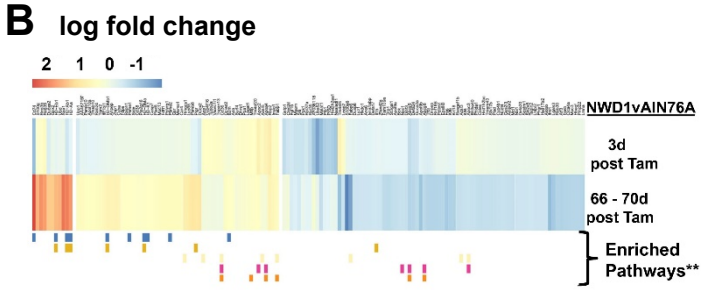

C **Enriched Pathways EC7, NWD1vAIN76A:
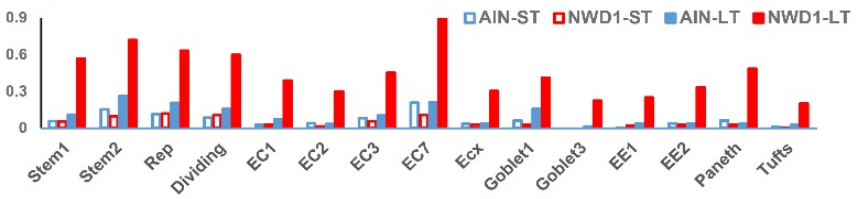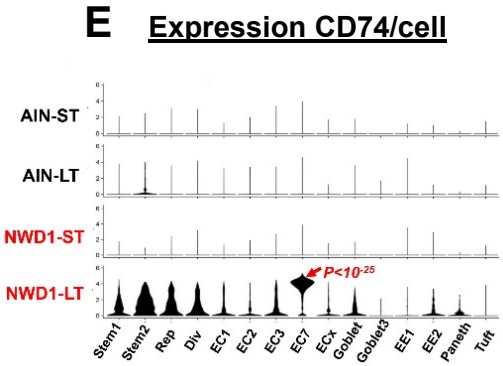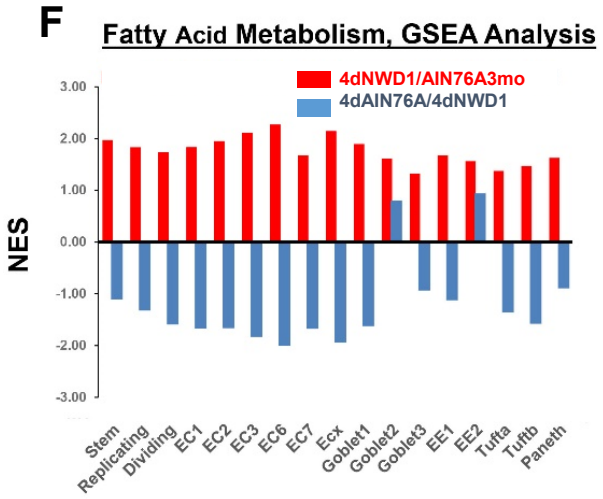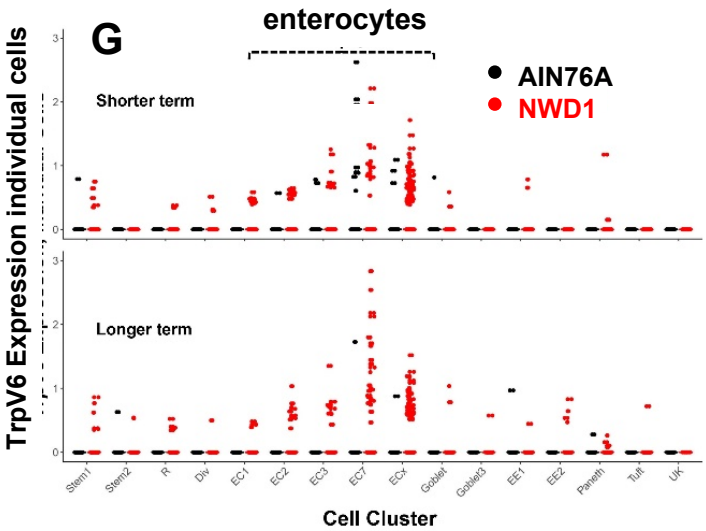
- antigen processing/presentation
- intestinal immune network, IgA production
- Ppar signaling
- cholesterol metabolism
- Fat digestion/absorption